NRC Research Press

ARTICLE

Stratigraphy and infill history of the glacially eroded Matane River Valley, eastern Quebec, Canada

Jean-Philippe Marchand, Thomas Buffin-Bélanger, Bernard Hétu, and Guillaume St-Onge

Can. J. Earth Sci. Downloaded from www.nrcresearchpress.com by Université du Québec à Rimouski on 01/02/14
For personal use only.

Abstract: Terraces in the lower Matane River Valley (eastern Quebec, Canada) were studied to describe the stratigraphic architecture of a glacially eroded valley fill. The Matane River Valley hosted a glacial tongue connected with a regional ice cap during the early opening of a calving bay in the modern St. Lawrence Estuary and was subsequently flooded by the Goldthwait Sea as the Laurentide Ice Sheet margin retreated. Stratigraphic, sedimentological, light detection and ranging (LIDAR), and geochemical analyses as well as radiocarbon measurements allowed the identification of four stratigraphic units deposited during and following deglaciation: glacial outwash (unit I), delta bottomsets (unit II), delta foresets (unit III), and fluvial deposits (unit IV). Stable isotope (^{13}C) and C/N ratio values reveal the relative influence of the two end-members (algae and terrestrial plants) on organic matter sources between the stratigraphic units. Climate, major relative sea level fluctuations, and sediment yield are recognized as the main controls on depositional environments in glacially eroded valleys of the northern shore of the Gaspé Peninsula during the Holocene. This paper presents a model of the evolution of the Matane River Valley, which in many points is similar to existing conceptual fjord-valley fill models.

Résumé : Des terrasses dans la partie aval de la vallée de la rivière Matane (Est du Québec, Canada) ont été étudiées dans le but de décrire l'architecture stratigraphique d'une vallée érodée par les glaciers. La vallée de la rivière Matane a abrité une langue glaciaire qui était reliée à une calotte glaciaire régionale durant l'ouverture précoce d'une baie de vêlage dans l'estuaire moderne du fleuve Saint-Laurent. La vallée fût par la suite inondée par la mer de Goldthwait à mesure du retrait de l'Inlandsis laurentidien. Des analyses stratigraphiques, sédimentologiques, géochimiques et par LIDAR (détection et télémétrie par ondes lumineuses) ainsi que des mesures au carbone 14 ont permis l'identification de quatre unités stratigraphiques déposées durant et après la déglaciation : des dépôts d'épandage fluvioglaciaire (unité I), des lits basaux de delta (unité II), des lits frontaux de delta (unité III) et des dépôts fluviaux (unité IV). Des valeurs d'isotopes stables (^{13}C) et de rapport C/N révèlent l'influence relative des algues et des plantes terrestres sur les sources de matière organique entre les unités stratigraphiques. Le climat, les grandes fluctuations relatives du niveau de la mer et les sources de sédiments constituent les principaux contrôles sur l'environnement de déposition dans les vallées érodées par les glaciers sur la rive nord de la péninsule gaspésienne durant l'Holocène. Cet article présente un modèle de l'évolution de la vallée de la rivière Matane, laquelle ressemble en plusieurs points aux modèles conceptuels existants de vallées de fjords.

Introduction

Alluvial systems are the scene of major environmental changes during glacial–interglacial transitions (Abreu and Anderson 1998). Streams fed from glacier melt display highly variable flows and sediment discharges, filling the deglaciated valley with variable successions of glacial, fluvioglacial, and fluvial deposits. During deglaciation, glacio-isostatic and eustatic sea-level rise cause flooding at the downstream end of valleys that induces sedimentation of terrestrial and marine origin. The subsequent drop in sea level causes the progradation and incision of the alluvial system and the formation of terraces (Fisk 1944; Blum and Törnqvist 2000). These terraces are of primary interest because their sedimentary records contain the high-resolution sequence of environmental changes.

Studies suggest a sharp contrast in alluvial processes between formerly glaciated and non-glaciated settings during a glacial–interglacial transition (Hansen 2004; Corner 2006). In fjords, most sedimentation occurred during forced regression, and the transgression system tract is usually thin or absent because invasion of the fjord proceeds while the glacier retreats during a relative drop in sea level. Numerous studies carried out in fjord valleys from Norway and Greenland (Hansen 2004; Corner 2006; Eilertsen et al. 2006, 2011; Hansen et al. 2009; Forwick and Vorren 2011) illustrate how detailed stratigraphic analysis can be used to extract paleoenvironmental information contained in deglaciated valleys.

This paper describes the evolution of a glacially eroded valley located in an area of major glacio-isostatic changes in the St. Lawrence Estuary, eastern Canada. We examined the stratigraphy of terraces that emerged during the Holocene within the lower Matane River Valley using an integrated multidisciplinary approach involving high-resolution morphostratigraphic imaging (light detection and ranging (LIDAR)), chronostratigraphy, and elemental (C, N) and stable isotope ($\delta^{13}C$) analysis. The main objectives of this study are to (*i*) define the main controls of the spatial

Received 5 April 2013. Accepted 13 October 2013.

Paper handled by Associate Editor Alan Trenhaile.

J.-P. Marchand* and T. Buffin-Bélanger. Laboratoire de géomorphologie et dynamique fluviale, Module de géographie, Centre for Northern Studies (CEN), Université du Québec à Rimouski, 300, allée des Ursulines, Rimouski, QC G5L 3A1, Canada.
B. Hétu. Module de géographie, Université du Québec à Rimouski, 300, allée des Ursulines, Rimouski, QC G5L 3A1, Canada.
G. St-Onge. Canada Research Chair in Marine Geology, Institut des sciences de la mer de Rimouski (ISMER) and GEOTOP Research Center, 310, allée des Ursulines, Rimouski, QC G5L 3A1, Canada.

Corresponding author: Jean-Philippe Marchand (e-mail: jp_kebec@hotmail.com).
*Present address: 2651 Bélair Street, Montréal, QC H2A 1Z9, Canada.

Can. J. Earth Sci. Downloaded from www.nrcresearchpress.com by Université du Québec à Rimouski on 01/02/14
For personal use only.

organization of the depositional elements in the valley during and following the deglaciation, (*ii*) compare the stratigraphy of the lower Matane River Valley with other fjord-valley fill models (Hansen 2004; Corner 2006), and (*iii*) discuss the application of the Matane River Valley fill model to neighbouring valleys on the northern Gaspé Peninsula.

Regional setting

The Matane River Valley lies on the northwest portion of the Gaspé Peninsula, in eastern Quebec, Canada (Fig. 1). The Gaspé Peninsula is made of extensively deformed sedimentary rocks associated with the Appalachian orogenesis from the Cambro-Ordovician period (Ollerenshaw 1967). The U-shaped Matane River Valley cuts into the Appalachian plateau with subrounded summits ranging between 100 and 350 m above sea level (a.s.l.). Upstream from the 60 km, the river flows in a mountainous area, the Notre-Dame mountain range, with a narrow valley and steeper river gradients. The Matane River is confined within older fluvioglacial sediments and locally by rock outcrops. The width of the valley floor ranges between 0.4 and 1.5 km, and the average river gradient is 0.19% (or 1.9 m/km). In the last 3 km, the river flows through a short coastal plain bordering the St. Lawrence Estuary.

Deglaciation model of the Matane River Valley

The current model of glaciation–deglaciation suggests that the Matane River Valley was repeatedly occupied by glaciers during the Wisconsinian period (110–10 ka BP). The Laurentide Ice Sheet expanded south of the present-day St. Lawrence Estuary and penetrated the western portion of the Gaspé Peninsula. Global eustatic sea level rise around 14 000 years BP triggered the opening of a calving bay in the axis of the present St. Lawrence Estuary, dividing the Laurentide Ice Sheet and isolating a regional ice cap centered on the Gaspé Peninsula (Dionne 1977). The calving bay reached the mouth of the Matane River Valley around 15 800 ± 1400 cal. years BP (Lebuis and David 1977), which triggered the deglaciation of the valley. The glacier tongue was then an extension of the regional Gaspé ice cap. The glacier tongue was anchored at the margin between the coastal plain and the Appalachian plateau, leading to the formation of a frontal moraine and a large subaquatic ice-contact wave-delta (Coll 1994). Coll (1994) dated deposition of the foreset beds of the ice-contact delta at 14 840 ± 720 cal. years BP (UL-873). Coll (1994) also interpreted the highest terrace levels in the inner valley as kame delta and kame terraces accumulated by glacial meltwater streams (Fig. 2).

Dionne and Coll (1995) and Hétu (1994) proposed that the waters of the Goldthwait Sea reached approximately 105–110 m a.s.l. in the Matane region. Dionne and Coll (1995) fixed the upstream limit of the sea invasion within 10–12 km of the current river mouth. A *Balanus* sp. shell found by Coll (1994) at the surface of the valley wall, dated to 12 885 ± 218 cal. years BP sets the maximum altitude of the former sea level in the valley at 70 m.

Methods

LIDAR and aerial photographs

Geomorphology was interpreted from high-resolution LIDAR images and orthorectified aerial photographs (1:20 000). Data coverage included the lower 40 km of the Matane River Valley. LIDAR images were computed to a final resolution of 1 m^2. Identification of the main morphological features was done with support from previous Quaternary studies and geological reports on the Matane region. We used ArcGIS (ESri) spatial analysis tools to calculate altitude, surface area, and slope. Terrace segments were delineated if their morphological features included a horizontal to semi-horizontal surface that was at least 100 m^2 and bounded by a distinct slope.

Stratigraphy and sedimentology

Stratigraphic and sedimentological information were used to characterize the selected terrace deposits. Terraces were selected on the basis of the estimated areal extent of the Goldthwait Sea invasion (Dionne and Coll 1995) within the valley and available outcrop exposures. Sediment samples were collected and analyzed for their coarse fraction (2–100 mm) using a sieving column and for their fine fraction (63–2000 μm) using a laser diffraction particle size analyzer (Beckman Coulter, model LS 13320). The grain size nomenclature is based on the modified Wentworth (μm) grade scale (Blott and Pye 2001). Dip and orientation of major bedding planes were measured in the field. Lithofacies were characterized using a coding scheme inspired from Heinz et al. (2003) and Miall (1978).

Dating and calibration

Previously published ages used in this study had been obtained by radiocarbon dating, but most of them were not calibrated. One single new date was acquired from a sample (ULA-3041) of wood (*Picea* sp.). This sample was dated at the Keck Carbon AMS Facility at the University of California and normalized to a $\delta^{13}C$ value of –25‰. All ages were calibrated (cal. years BP) using the Calib Rev 6.1.0 online software using either the Intcal09 or Marine09 calibration curves for terrestrial samples or marine carbonates, respectively. Following Occhietti and Richard (2003), a $\delta^{13}C$ value of –25‰ for terrestrial samples and 0‰ for marine samples was estimated when the $\delta^{13}C$ value was unknown, as was the case for the oldest results. For marine samples, it resulted in a 410 year correction before calibration. An average ΔR (reservoir age) of 123 ± 90 years was then applied to the marine carbonate samples based on the available data for the Matane region (McNeely et al. 2006). Table 1 lists all reported ages used in this study. The relative sea level curve from Dionne and Coll (1995) was converted to calibrated ages (Fig. 3).

Geochemical and stable isotope analyses

Carbon (C) and nitrogen (N) contents were measured in the sediments, and the $\delta^{13}C$ of the sedimentary organic matter was analyzed. The organic carbon to total nitrogen ratio (C/N) and the stable isotope ratios were used as additional tools for the reconstruction of paleoenvironments in the lower Matane River Valley. Combined, these analyses allow the distinction of paleo-aquatic environments based on the nature of the organic matter (e.g., Meyers 1997; St-Onge and Hillaire-Marcel 2001; Wilson et al. 2005).

Samples were first sieved at 63 μm to measure only the fine fraction to reduce possible variations between different units based on grain size (Meyers 1997). The fine fraction then underwent a triple HCl 10% (*v*/*v*) attack to remove carbonates and thereby isolate the organic carbon. Between 5 and 7 mg of treated samples were then rinsed, dried, crushed, and encapsulated in tin wells. Standards were also encapsulated to create a calibration curve for the $\delta^{13}C$. The standards used were caffeine (–33.79‰), microalgae (*Nanochloropsis*; –18.60‰), and Mueller Hinton Broth (–24.31‰). Stable isotope analyses were performed with a ThermoFinnigan Delta plus XP mass spectrometer. The $\delta^{13}C$ data are reported per mil (‰) rather than Vienna Pee Dee belemnite (VPDB) standard. The analytical error on measurements (number of samples $n = 50$) was 0.4‰ and 0.2‰ for δC and δN, respectively. System suitability prior to analysis was evaluated using standard deviation of zero reference gas (nitrogen and carbon dioxide) over 10 measurements, and the maximum acceptable variation was set to 0.06‰.

Results

Description and interpretation of morphology

Our detailed analysis of LIDAR images allowed the identification of 91 terrace segments in the valley within 20 km of the current river mouth. Figure 2 shows the terrace segments on the

Fig. 1. Maps showing the location of the Matane River Valley and the morphology of surface deposits within 10 km of the current river mouth (modified from Coll 1994).

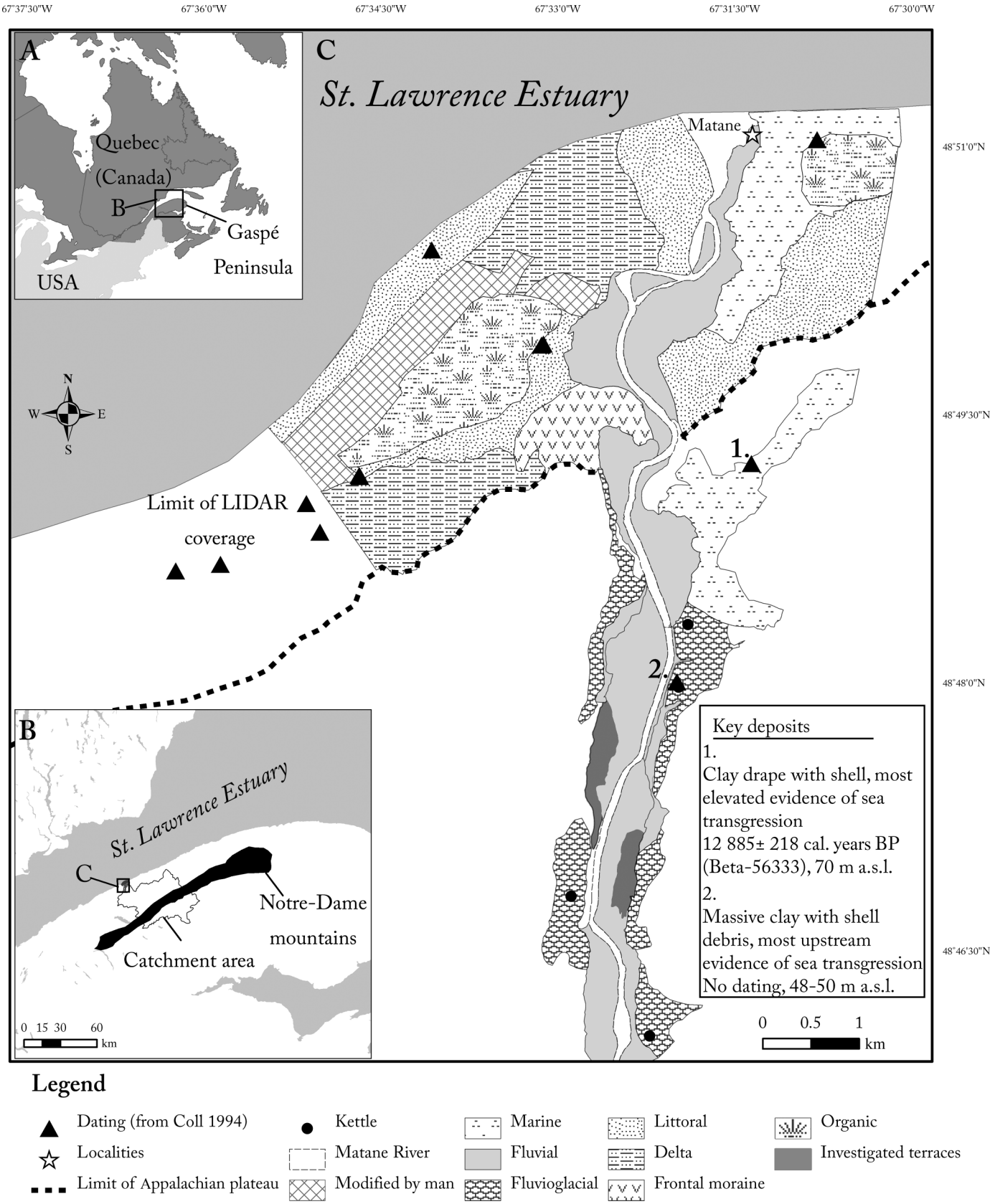

Can. J. Earth Sci. Downloaded from www.nrcresearchpress.com by Université du Québec à Rimouski on 01/02/14
For personal use only.

Can. J. Earth Sci. Downloaded from www.nrcresearchpress.com by Université du Québec à Rimouski on 01/02/14
For personal use only.

Fig. 2. Terrace surfaces located in the lower Matane River Valley classified by genetic type. (A) LIDAR coverage with mapped terrace surfaces; (B) maximum altitude of terrace surfaces shown in the longitudinal profile. (See colour in online version.)

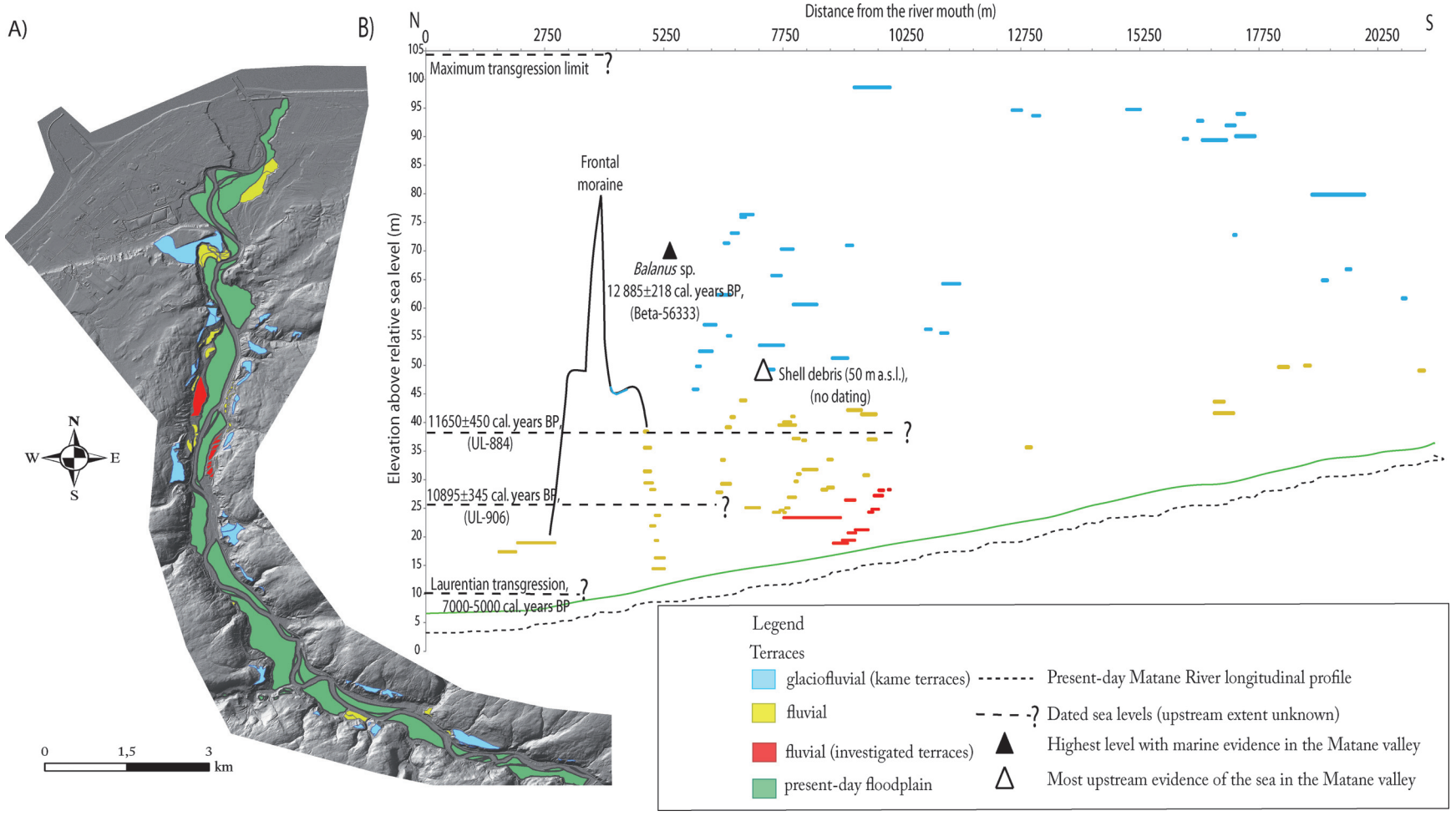

Table 1. Radiocarbon ages with calibration.

Lab	Reported ^{14}C ages ($\delta^{13}C$ = 0‰)	Conventional ^{14}C ages ($\delta^{13}C$ = −25‰)	Material or species	Calibrated age BP (minimum)	Calibrated age BP (maximum)	Relative area (%)	Altitude a.s.l. (m)	Source
QU-84	13450±470	13860±470	*Hiatella arctica*	14458	17256	98	—	Lebuis and David 1977
ULA-3041	4115±20	4115±20	Wood (*Picea* sp.)	4529	4809	100	—	Present paper
Beta-55214	—	3640±60	Wood	3828	4103	96	—	Dionne and Coll 1995
UL-979	5760±80	5760±80	Wood	6398	6743	99	—	Dionne and Coll 1995
UL-2156	3670±70	3670±70	Wood	3831	4164	97	—	Hétu and Gray 2000
Beta-13854	—	4410±80	Wood	4851	5288	100	—	Gray and Hétu 1987
UL-1572	2990±80	3400±80	Mixed shells	2799	3382	100	—	Gray and Hétu 1987
Beta-56333	—	11530±120	*Balanus* sp.	12667	13102	100	70	Coll 1994
UL-1348	11520±150	11930±150	*Mytilus edulis*	12882	13675	100	60	Dionne and Coll 1995
UL-972	10320±130	10730±130	*Mytilus edulis*	11266	12381	99	53	Coll 1994
Beta-56334	—	10410±140	Mixed shells	10881	11963	99	50	Coll 1994
Beta 56335	—	9660±90	*Macoma balthica*	10131	10658	100	49	Coll 1994
UL-860	10720±110	11130±110	Mixed shells	12040	12770	100	46	Coll 1994
UL-788	10740±140	11150±140	*Mytilus edulis*	12008	12886	100	45	Coll 1994
UL-873	12750±130	13160±130	Mixed shells	14123	15556	100	39	Coll 1994
UL-884	10180±110	10590±110	Mixed shells	11193	12105	100	38	Coll 1994
Beta 56336	—	11260±100	Mixed shells	12280	12951	100	33	Coll 1994
UL 926	6900±190	6900±190	Peat	7428	8055	98	33	Coll 1994
UL 906	9580±140	9580±140	Wood	10550	11238	99	26.5	Coll 1994
UL-861	9500±100	9910±100	Mixed shells	10398	11105	100	26	Coll 1994
UL-820	8020±90	8020±90	Peat	8603	9127	100	23	Coll 1994
UL-795	10350±140	10760±140	Mixed shells	11306	12403	97	20	Coll 1994
Beta-52526	—	4440±60	Peat	5096	5144	99	18	Coll 1994
UL-814	8170±110	8170±110	Peat	8846	9438	96	17	Coll 1994
UL-836	8910±100	9320±100	Mixed shells	9550	10268	100	16.8	Coll 1994
UL-903	8190±80	8190±80	Peat	8996	9407	100	16	Coll 1994
UL-793	6860±90	6860±90	Peat	7570	7869	97	16	Coll 1994
Beta-52525	7870±60	7870±60	Peat	8544	8977	100	15	Coll 1994
UL-979	5760±80	5760±80	Wood	6398	6743	99	6.7	Coll 1994
Beta-56332	—	4910±90	Mixed shells	4782	5427	100	4	Coll 1994
UL-900	4830±70	4830±70	Wood	5328	5717	100	3.8	Coll 1994
Beta-56331	—	4790±100	Mixed shells	4551	5279	100	3.7	Coll 1994
UL-984	4700±80	4700±80	Wood	5287	5600	99	3.8	Coll 1994
UL-899	4310±70	4310±70	Wood (*Picea* sp.)	4627	5056	97	5.8	Coll 1994
UL-874	4300±80	4300±80	Wood	4607	5064	95	3.9	Coll 1994
UL-980	4270±80	4270±80	Wood	4568	5046	99	6.6	Coll 1994
Beta-55213	—	4170±60	Wood	4566	4842	96	3.8	Coll 1994
UL-973	4100±80	4100±80	Wood	4431	4828	100	6.4	Coll 1994
UL-982	4080±90	4080±90	Wood	4405	4842	99	4.1	Coll 1994
Beta-55215	—	4000±70	Wood	4245	4806	100	4.1	Coll 1994
UL-972	4000±70	4000±70	Wood	4245	4806	100	5.4	Coll 1994
Beta-55214	—	3640±60	Wood	3778	4148	100	5.1	Coll 1994
UL-938	2170±70	2170±70	Wood	2002	2333	100	6.1	Coll 1994
UL-905	1000±60	1000±60	Wood (*Picea* sp.)	778	1055	100	7.2	Coll 1994
Beta-55212	—	4010±60	Wood	4294	4804	100	5.4	Coll 1994
TO-4559	—	4270±60	Wood	4617	4976	98	3.8	Dionne and Coll 1995
UL-891	1520±80	1520±80	Peat	1289	1566	100	7.4	Dionne and Coll 1995
QU-146	2380±90	2790±90	Mixed shells	2061	2705	100	7	Lebuis and David 1977
QU-152	2260±110	2670±110	*Mya* sp.	1872	2610	99	6	Lebuis and David 1977
TO-4305	—	2250±40	*Mesodesma* sp.	1476	1951	100	6.6	Dionne and Coll 1995
UL-858	1830±70	2240±70	*Mesodesma* sp.	1415	1961	100	6.5	Dionne and Coll 1995

Note: For Beta (Beta Analytic, Miami, Florida) and TO (University of Toronto, Ontario), $\delta^{13}C$ values adjusted to −25‰; for QU, UL, and ULA (Université Laval, Québec, Quebec), $\delta^{13}C$ values not adjusted to −25‰. a.s.l., above sea level.

basis of their maximum height above sea level alongside a longitudinal valley profile. The high-lying terrace segments are observed over the full length of the valley and lie between 31 and 80 m above the modern plain. These terraces can be identified from both the occurrence of depressions at their surface as well as their irregular margin morphology on the LIDAR digital elevation model (DEM) (Fig. 4). Their surface areas vary from 1170 to >300 000 m^2 and their slope from 6% to 0.1%, and they are oriented mostly perpendicular to the valley axis. The lower-lying terrace segments occur between 1 and 41 m above the modern plain. They have narrow tread, are not paired, and their dissected surfaces are associated with incised tributaries. The edges of these terraces are mostly regular, either straight or curved.

The investigated terraces are located at a low elevation above the modern plain and occupy a large surface area (Fig. 4). They occur within 8–10 km of the river mouth, 5 km south from the municipality of Matane and rise between 20 and 28 m above current sea level. The terrace on the west side exhibits a large uniform surface 6.5 m above the modern plain and has a moderate gradient (1.45%). The terraces on the east side show nine levels displayed in staircase morphology with a downstream orientation. The most upstream and downstream levels are, respectively,

Can. J. Earth Sci. Downloaded from www.nrcresearchpress.com by Université du Québec à Rimouski on 01/02/14
For personal use only.

Can. J. Earth Sci. Downloaded from www.nrcresearchpress.com by Université du Québec à Rimouski on 01/02/14
For personal use only.

Fig. 3. Sea-level curve from the Matane region with calibrated ages (modified from Coll 1994).

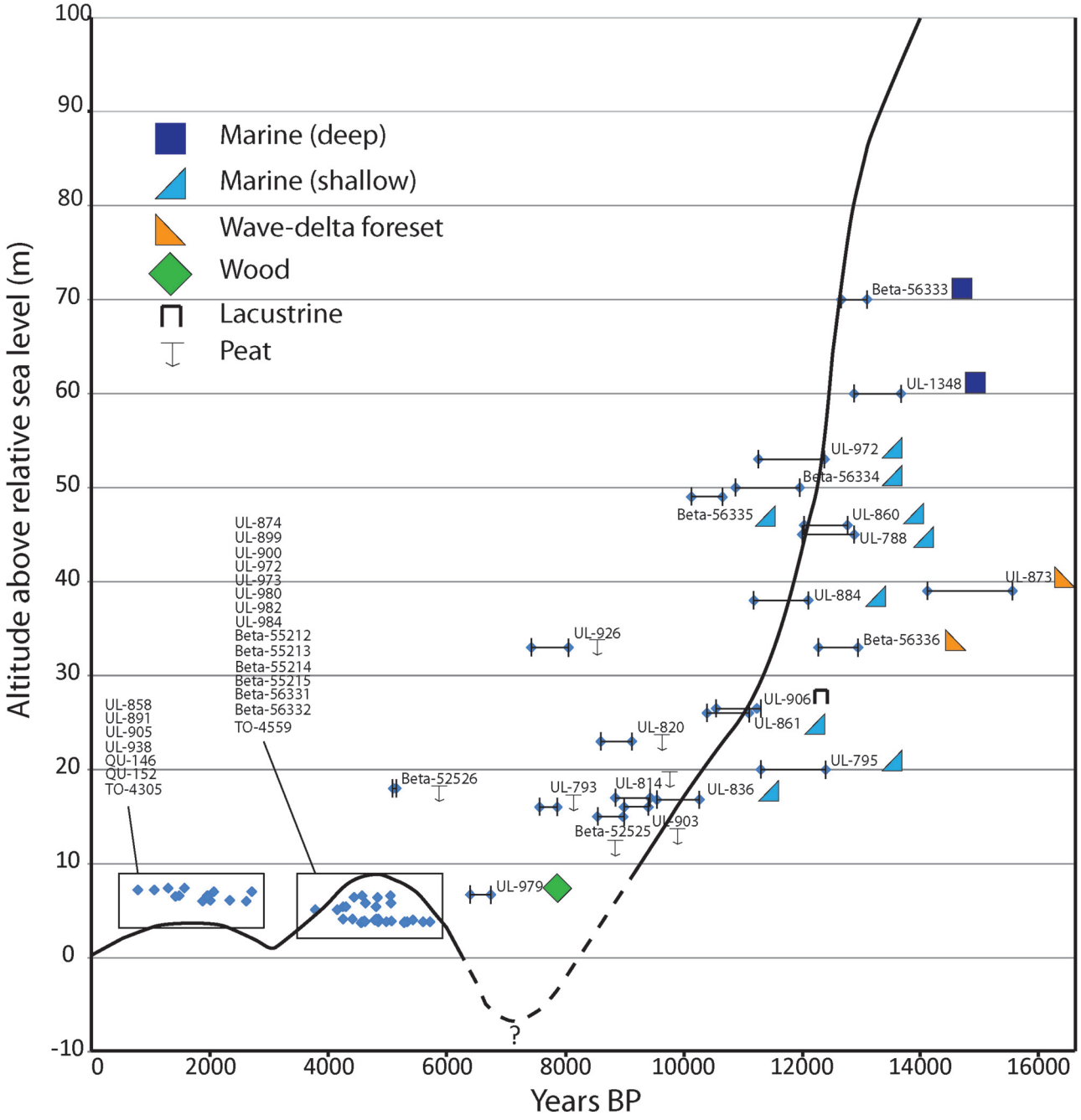

9.5 and 1 m above the modern plain. The gradient of the east side terraces ranges between 0.16% and 0.42%. Relict channel forms are observed on the surfaces of each level.

The same fluvial features are observed at the surface of the modern plain (Fig. 4). Abandoned channels >2.5 m deep are present and form a braided pattern with relict longitudinal bars. Some relict bars are also dissected by multiple small channels, giving rise to complex bar morphology.

Interpretation

The high-lying terraces are interpreted as kame terraces based on the presence of shallow depressions at their surface, interpreted as kettle, and their irregular margin morphology, which is associated with ice melt. Coll (1994) described inclined strata with marked grain-size variations in those terraces, which she interpreted as juxtaglacial deposits. The second series of terraces was interpreted by Coll (1994) to have fluvial origin, although no stratigraphic evidence was presented. The regular margin morphology of these terraces suggests flow erosion, while the unpaired configuration indicates fast incision rates. The complex bar morphology at the surfaces of the investigated terraces indicates a multiple-channel fluvial environment.

Description and interpretation of stratigraphic units

Three and five sections, between 2 and 8 m wide, were studied from the west (W1–W3) and east (E5–E9) terrace, respectively (Fig. 4). One pit hole was hand-excavated directly in the modern plain (FP4). Four units are characterized and interpreted on the basis of lithofacies association, geometry, their relative position

Can. J. Earth Sci. Downloaded from www.nrcresearchpress.com by Université du Québec à Rimouski on 01/02/14
For personal use only.

Fig. 4. High-resolution digital elevation model with investigated terraces and main geomorphological features of the Matane River Valley (Kt, kame terrace; Fl, fluvial terraces). Relict channel forms can be observed at the surface of the right terrace and the modern floodplain (dashed lines). Stratigraphic sections are identified with white triangles (numbered from 1 to 9 in an upstream direction). The vertical exaggeration of ground elevation is three.

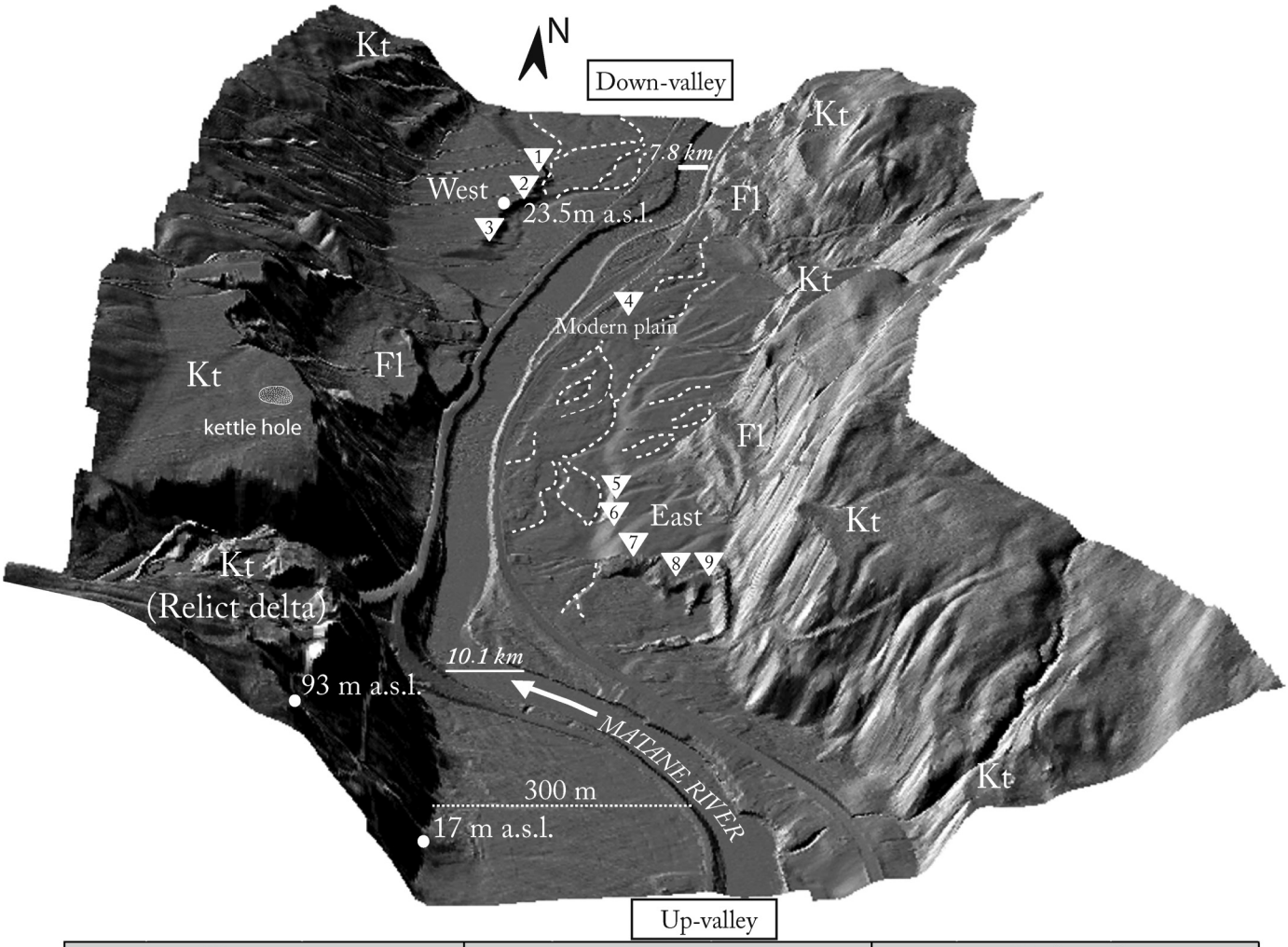

West terrace			East terrace			Modern plain		
Section	Lat.	Long.	Section	Lat.	Long.	Section	Lat.	Long.
W1	48° 47' 42.3636"	-67° 32' 30.4836"	E5	48° 46' 53.7636"	-67° 32' 29.7702"	MP4	48° 47' 10.6836"	-67° 32' 29.385"
W2	48° 47' 40.9236"	-67° 32' 29.7702"	E6	48° 46' 51.963"	-67° 32' 30.1272"			
W3	48° 47' 35.1528"	-67° 32' 33.7272"	E7	48° 46' 46.1964"	-67° 32' 29.385"			
			E8	48° 46' 43.6836"	-67° 32' 26.1744"			
			E9	48° 46' 42.9558"	-67° 32' 26.1744"			

in the valley, and age based on radiocarbon dating. Nine lithofacies were defined to describe the different units (Table 2).

Unit I: glacial outwash

Unit I is observed in section E8, between 19 and 21 m a.s.l. (Fig. 5). Unit I sits on a highly polished shale bedrock with irregular morphology. This unit is characterized by inclined beds (13°–21°), roughly dipping up-valley (towards the east-southeast), and consists of stratified and graded gravel with a bimodal grain size composition (facies 6). Some layers contain so little fine matrix as to be openwork. Angular to subrounded blocks are embedded in a silt matrix (Fig. 5D). The limited exposure makes it difficult to characterize the external form of the deposit. The upper contact to unit II is conformable (Fig. 5).

Interpretation

Stratified graded gravel beds may be associated with bars in a fluvial channel (Miall 2006), but the alternation between matrix-rich gravel and openwork gravel beds is unusual in a purely fluvial setting (Shaw and Gorrell 1991). Matrix-rich gravel results from bedload transport over an avalanching slope and suspension load deposition from return flow. The openwork gravel is associated with maximum bedload transport rates. In flow with shear velocities well above critical values, large clasts have higher velocities than small clasts, which leads to strong sorting and creates an openwork texture (Shaw and Gorrell 1991). Graded bimodal gravel has been reported in glaciofluvial and subglacial deposits (Sandgren 1983; Veillette 1986; Fiore et al. 2002). Several other observations could indicate intense flows near glacier ice. For

Table 2. Lithofacies characterization and interpretation.

Facies	Lithology	Description	Interpretation
1. Matrix-supported, stratified sand and gravel	Medium sand to small gravel, poorly sorted (4.8). G: 28%–84%, S: 15%–66%, M: 2%–18%.	Beds dip (10° to 35°). Stratification originates from change in grain size. Beds range from 2 to 100 mm in thickness, and contacts are conformable.	Main depositional agent was sediment gravity flows on a slope (Nemec 1990). Variation in the proportion of gravel implies that the water to sediment ratio was fluctuating from flow to flow (Kostic et al. 2005).
2. Matrix-supported, gravel and sand with grading	Coarse sand to medium gravel, poorly sorted (2.5). G: 2%–78%, S: 18%–95%, M: 3%–9%.	Beds show crude horizontal stratification. Sets are differentiated by normal to inverse grading. Larger clasts are imbricated. Beds are 10–100 cm thick.	Horizontal bedding and the sand matrix indicates deposition in the form of bedload sheets under the lower flow regime. The imbrication of large clasts suggests bedload transport during peak discharge. Inverse and normal grading reflect fluctuation of flow during deposition.
3. Matrix-supported, trough cross-stratified sand and gravel	Coarse to fine sand with variable proportions of gravel, well sorted (1.49). G: 22%–42%, S: 34%–77%, M: 2%–24%.	Trough cross-stratified beds. Each set is between 1 and 5 cm thick.	Trough cross-stratification are caused by the migration of three-dimensional dunes with sinuous-shaped crest, that implies turbulent flows (Miall 2006). Good sorting implies a hydraulic sorting by a continuous flow in a channel (Miall 2006). Occurrence of fine lamina and some oversized clasts indicate variable flow.
4. Imbricated clast-supported gravel	Coarse gravel and small cobble, very poorly sorted (6.37). G: 67%, S: 31%–22%, M: 2%–11%.	Open framework with crude stratification. Clasts are imbricated and defined subhorizontal beds between 10 and 100 mm thick. Beds are dipping at angle between 0° and 14°.	Imbrication and horizontal bedding implies transportation of gravel in planar sheets, which would be expected in very high competent flow (Rust 1972). Deposition occurred rapidly, as suggested by the lack of sorting and poorly defined bedding (Kostic et al. 2005).
5. Clast-supported, stratified gravel, and cobble	Coarse sand, gravel, and cobble, very poorly sorted (5.9). G: 77%–84%, S: 12%–22%, M: 1%–5%.	Openwork gravel composed of well-imbricated clasts, dipping in multiple directions. Beds are between 200 and 500 mm thick. Contacts are erosional. Sets randomly show normal grading and are marked locally by boulder lines.	Imbrication refers to tractional transport in powerful flow and deposition in the form of bedload sheets on fluvial bar or into the channel (Hein and Walker 1977). Strata dipping in opposite direction might refer to accretion on middle bar (Lunt et al. 2004). Overall, the grain size and grading between individual gravel beds suggests highly variable flow. Boulders may represent lag deposit during flood stage.
6. Graded, bimodal gravel	Coarse gravel, poorly sorted (2.5) with fine matrix, poorly sorted (2.5). G: 85%, M: 15%.	Openwork gravel interlayered with matrix-supported gravel. Clasts are imbricated and defined subhorizontal beds between 5 and 30 cm thick. The coarse clasts show normal grading. Beds are dipping at angle between 5° and 22°.	The imbricated gravel beds suggest bedload deposition in unidirectional flows. The grading implies pulses of sediment transport and deposition. Matrix-rich gravel results from bedload transport over an avalanching slope and suspension load deposition from return flow (Shaw and Gorrell 1991).
7. Massive fine sand	Very coarse silt to coarse sand, poorly sorted (3.9). It contains a variable amount of sand (between 36% and 87%) and mud.	No apparent bedding. The deposit reaches between 0.6 and 1.2 m in thickness.	Massive fines refer to gravity-flow deposition during waning stage of floods. The poor sorting suggests rapid deposition, while the lack of structure could come from the reworking of deposits by the next episode of flooding.
8. Stratified sand	Fine to coarse-grained sand, poorly sorted (3.05). Larger clasts, subrounded to angular, are occasionally embedded. Sand: 58%–95%, silt: 4%–39%, clay: 1%–3%.	Horizontal bedding, alternating beds of coarse to medium sand grading into fine sand with lower erosional contact. Graded bed thickness varies between 100 and 400 mm. Wavy beddings and small ripples are visible locally. Many internal synsedimentary deformations are displayed.	Graded bedding and occurrence of coarse sand refer to deposition in a basin characterized by alternating phase of unsteady density flows (McCabe and Eyles 1988). Grading is induced by discharge variation (Eilersten et al. 2011). Oversized clasts are associated with ice-rafted debris. Wavy bedding results from traction current, modifying the surface of the newly deposited layer (Kostic et al. 2005).
9. Stratified fine sand and silt	Fine-grained sand and silt, poorly sorted (2.7). Sand: 0%–56%, silt: 41%–71%, clay: 3%–35%.	Horizontal bedding, alternating beds of fine silt grading into silt and clay, with lower erosional contact. Graded bed thickness varies between 2 and 10 cm.	Graded bedding and occurrence of silt and clay refer to deposition in a basin characterized by low density flows and suspension (McCabe and Eyles 1988). Grading is induced by discharge variation (Eilersten et al. 2011).

Note: Number in parentheses indicates sorting value. G, gravel; S, sand; M, mud (silt and clay).

Can. J. Earth Sci. Downloaded from www.nrcresearchpress.com by Université du Québec à Rimouski on 01/02/14
For personal use only.

Fig. 5. (A) Stratigraphic log from section E8; (B) photograph of the upper fluvial unit (unit IV) showing coset beds of stratified coarse gravel with varying orientation (facies 5) and lower erosive contact with unit III; (C) photograph of dipping erosional contact between the deltaic deposit (unit III) and prodeltaic graded beds (unit IV); (D) photograph of stratified coarse gravel (facies 6) with large subrounded clasts. Note the coarse gravel embedded in the silty matrix in the inset. (The legend on this figure also applies to Figs. 6, 8, and 9.) s, silt; p, pebble; c, cobble; b, boulder.

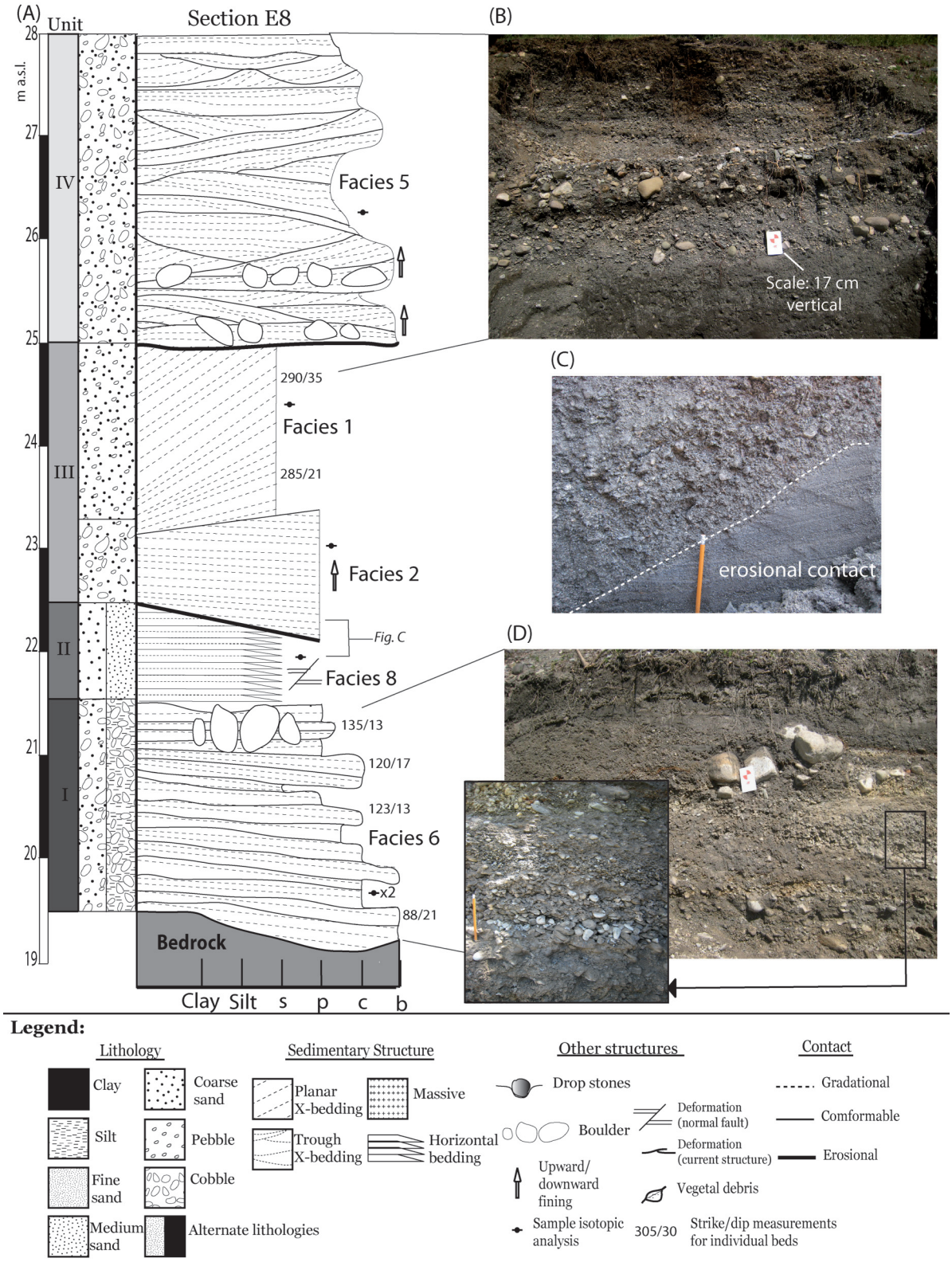

Can. J. Earth Sci. Downloaded from www.nrcresearchpress.com by Université du Québec à Rimouski on 01/02/14
For personal use only.

Fig. 6. Stratigraphic logs from sections (A) W2 and (B) E5. (C) Photograph of the erosional contact between the upper fluvial deposit (unit IV) and fine-grained graded deposits (unit II); the inset box shows the fine-grained layers with wavy bedding and variable thicknesses (facies 9). (D) Photograph of the massive sand deposits (facies 7) topping the bedload deposits. (E) Photograph of the stratified sand with oversized clast and tilted strata (facies 8). The lower contact between units IV and II is erosional and marked by boulder-size sediment lags. (See Fig. 5 for the legend.)

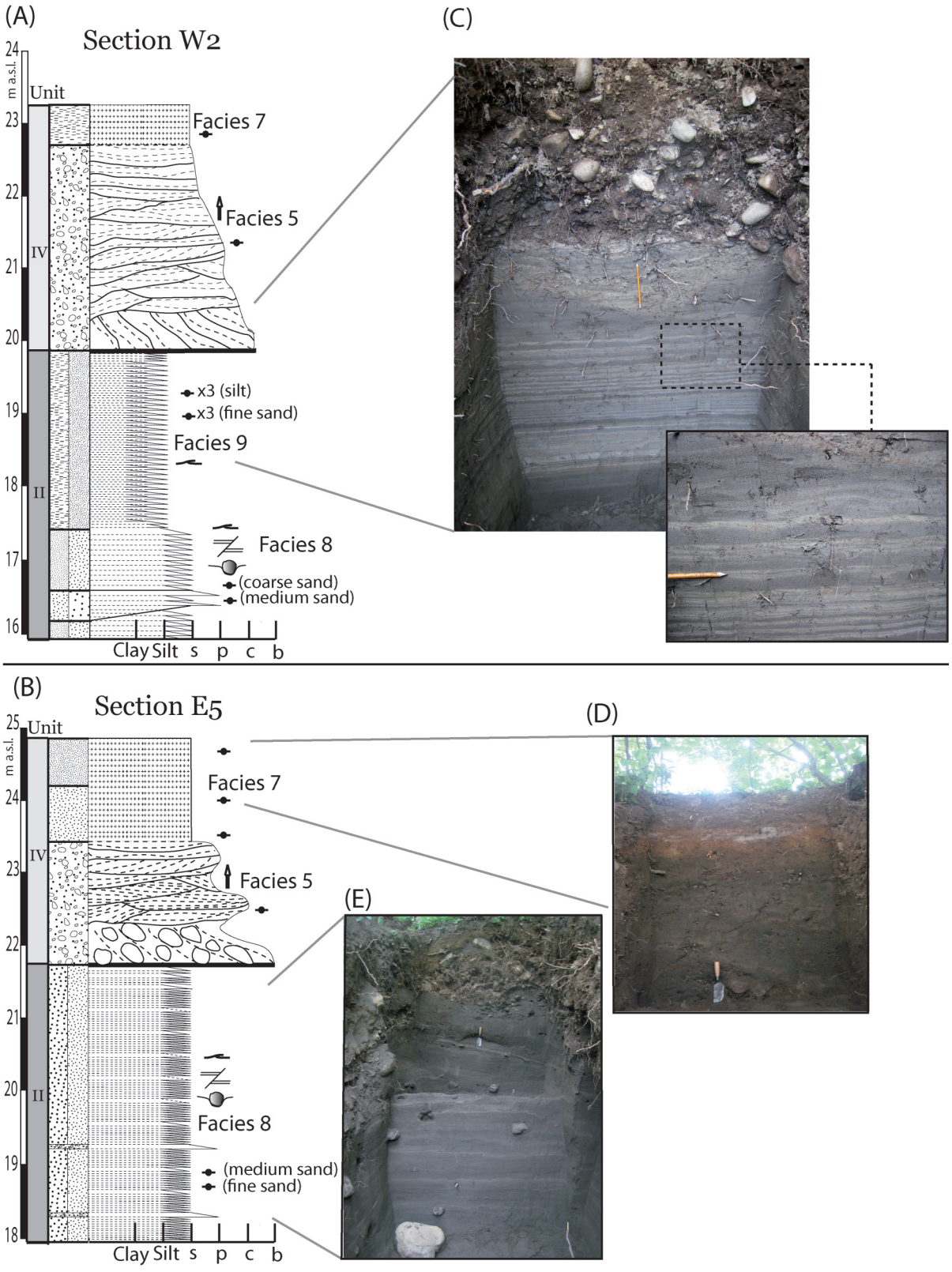

Can. J. Earth Sci. Downloaded from www.nrcresearchpress.com by Université du Québec à Rimouski on 01/02/14
For personal use only.

Fig. 7. Bedding structures and deformations in stratified sand (facies 8) from section W5. (A) Inverse fault and multi-layer couplets of medium to coarse sand grading in fine sand; (B) close-up of a small-scale inverse fault; (C) wavy bedding of the finest lamina; (D) dropstones and coarse-grained layers, interpreted respectively as ice-rafted debris and underflow deposits.

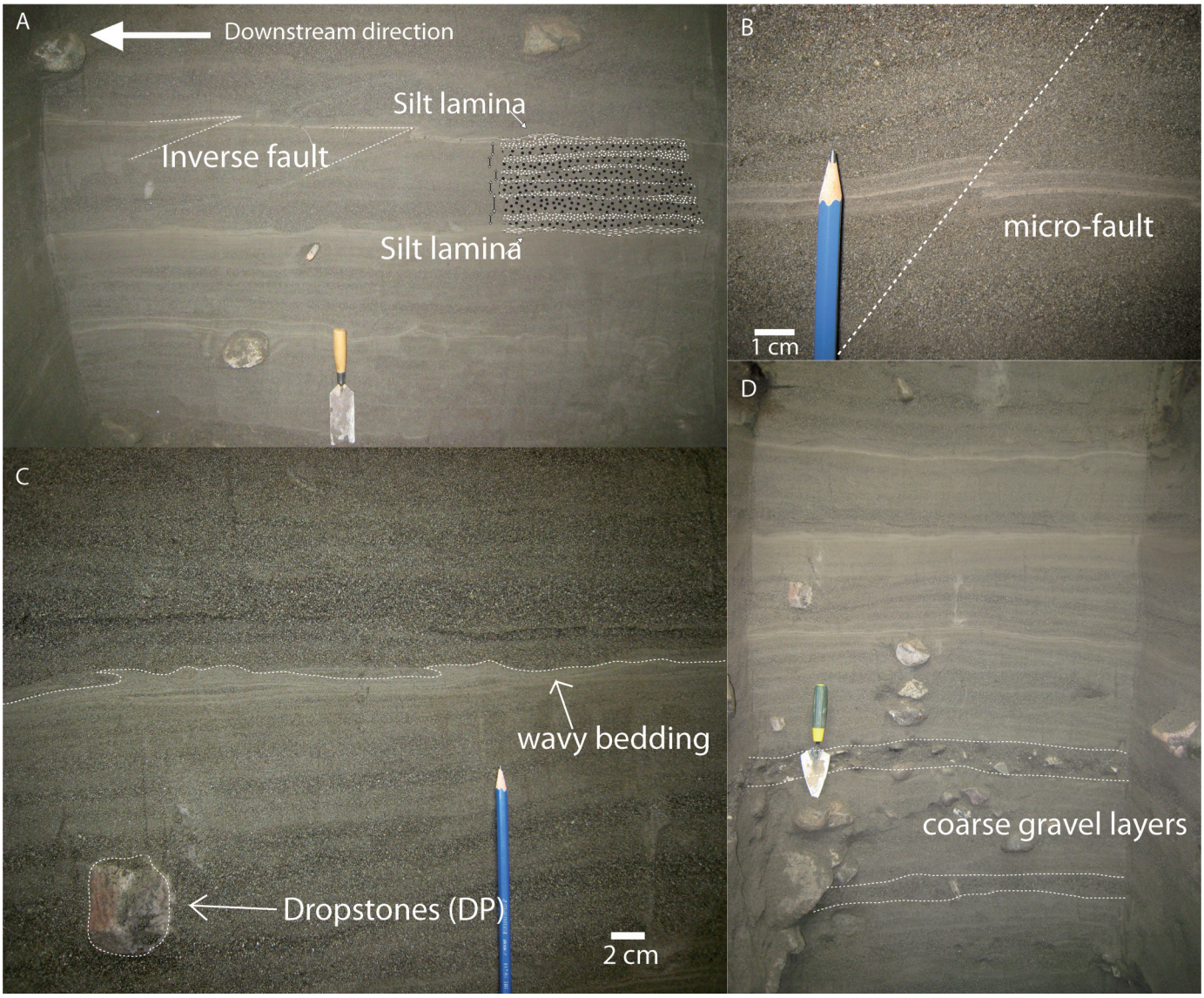

Can. J. Earth Sci. Downloaded from www.nrcresearchpress.com by Université du Québec à Rimouski on 01/02/14
For personal use only.

example, the angular blocks in the top of unit I reflect short transportation and could have melted out of glacier ice. Also, the up-valley orientation of stratification could indicate backset deposition. Backset deposition implies that the current was under high hydraulic pressure, like in bedrock-confined flow, and is reported from subglacial channel deposits (Fiore et al. 2002). Finally, basal contact with the polished valley bedrock suggests intense erosion prior to deposition. The upper contact with bottomset deposits (see unit II) indicates a drastic change from bedload to subaquatic sedimentation. Such transitions are well known from settings where deglaciation has occurred in a standing body of water like a fjord (Forwick and Vorren 2011). A gradual transgression would have resulted in a transitory facies between fully alluvial and subaquatic deposits (Miall 2010).

Unit II: delta bottomsets

Unit II is found in sections W1, W2, E5, and E8, and it also composes the substrate on which lies the fluvial bedload in the modern floodplain (section FP4). It encompasses two major lithofacies: stratified sand, graded, with horizontal bedding (facies 8) and stratified fine sand and silt, graded, with horizontal bedding (facies 9). The unit occurs between 14 and 23 m a.s.l., indicating a minimum thickness of 9 m. Unit II is likely the thickest unit of the valley fill in the investigated area. No other data currently exist on the depth of this unit or on the depth and shape of the bedrock. No fossil evidence was found in this unit during fieldwork.

In section W2, a 4 m high exposure allows us to describe the vertical succession of unit II (Fig. 6A). At the bottom of the section, medium to coarse sands grade into fine sand, forming graded beds averaging from 10 to 40 cm in thickness (facies 8). Subrounded clasts, between 5 and 20 cm in diameter, are isolated in the deposit. The deposit changes upwards into fine horizontal beds (facies 9) that show graded beds of very coarse silt grading into very fine silt. Layers from both facies display current structures such as wavy beddings and ripple formsets in the finest lamina. In section E5 (Fig. 6B) and W2, unit II is characterized by a few very coarse sand layers (facies 8) with a greater number of subrounded clasts than other sections.

Can. J. Earth Sci. Downloaded from www.nrcresearchpress.com by Université du Québec à Rimouski on 01/02/14
For personal use only.

Deformations are visible in all exposures of unit II but are only associated with facies 8 (Fig. 7). Throw between faults generally are a few centimetres high but can reach up to 40 cm. Several normal faults create graben-like structures. Small-scale reverse faults and tilted strata are also observed. In section E5, tilted strata dip in an up-valley direction (Fig. 6).

Interpretation

Unit II is interpreted as bottomsets in a glacio-deltaic or fluvio-deltaic environment. Graded beds are often associated with bottomsets in glacially fed deltas (McCabe and Eyles 1988; Corner et al. 1990; Eilertsen et al. 2011). The normal graded sand beds (facies 8) suggest that density flow was the main process of deposition in the basin (Chauvin 1977; Middleton 1993). By contrast, in glaciolacustrine varves, the couplet shows a sharp contact between the coarsest and finest beds resulting from two different deposition mechanisms (Ashley 1975; Benn and Evans 2010). Each graded bed from the Matane River sections, with its lower erosional contact, is interpreted as the A unit of the Bouma sequence (Bouma 1962), which is typically found in proximal turbidites (Middleton 1993) and produced by surge-type density flows and suspension settling (Eilertsen et al. 2011). Indeed, the abundance of coarse sand indicates a sediment source probably within <1 km (Corner et al. 1990; Corner 2006; Hansen 2004). Glacier meltwater streams or highly dynamic fluvial streams must have carried enough sediment to generate density flows in the basin.

Fine-grained graded beds (facies 9) were deposited by the action of low-density flows and suspension sedimentation from plumes. The transition between coarse-grained and fine-grained graded beds indicates a retreat of the sediment sources. The very coarse layers with great numbers of subrounded clasts (sections E5 and W2) represent episodic flood events (McCabe and Eyles 1988). Overall, unit II shows that the basin was under the influence of density flows that spanned a large range of scales.

The faults in unit II are interpreted as synsedimentary or post-depositional deformations, indicating fast sedimentation and poor consolidation (Pisarska-Jamrozy and Weckwerth 2012). Erosion by density flows can also destabilize the sediments (Pisarska-Jamrozy and Weckwerth 2012). Reverse faulting could be generated at the toe of a subaqueous landslide or could be generated by an iceberg keel (Longva and Bakkejord 1990). Numerous subrounded clasts embedded in the deposits reveal the activity of floating ice derived from glacier calving or from sea ice (McCabe and Eyles 1988). High sedimentation rates combined with major freshwater inputs could also explain the absence of macroscopic fauna in unit II (McCabe and Eyles 1988; Hansen 2004).

Unit III: delta foresets

Unit III consists of sand and gravel with either planar stratifications (facies 1) or graded with crude subhorizontal stratification (facies 2). The thickness of unit III varies between 6 and 1.5 m and ranges from 17 to 26 m a.s.l. The dip direction of planar beds is towards the northwest (280°–305°). Unit III is present in the three most upstream sections (E7–E9) and in sections E6, W3, and W1. The basal contact is visible in only two sections (E8 and W1). It overlies unit II with an oblique and erosional contact. The upper contact with unit IV is irregular and erosional.

Planar beds display various amount of gravel and various angles of dip, which vary between 4° and 31°. Steep planar beds are displayed upstream in section E7 (Fig. 8), while low-gradient planar beds are visible in sections E6 and W3 (Fig. 9). Average grain size and dip angle of planar beds generally decrease downstream.

The stratified sand and gravel beds with normal and inverse grading (facies 2) are found underneath stratified sand and gravel with planar bedding (facies 1). Facies 2 is also observed in truncated deposits in sections E9 and W1 (Fig. 9). In these three sections (W1, E8, and E9), the unit III deposits share a concave–oblique and erosional contact with unit II.

Interpretation

The planar beds with high dip angle found in section E7 are interpreted as deltaic foresets. Since the beds are at an angle of rest, deposition occurred on an avalanching slope (foreset) that gradationally or erosionally prograded over the basin floor (Nemec 1990; Hansen 2004). Planar beds with low dip angles are interpreted as distal foresets in a coarse-grained delta (delta toe). The average grain size and dip angle of foreset beds generally decrease downslope and indicate a typical proximal to distal relationship within the delta slope (Kostic et al. 2005; Benn and Evans 2010). These distal beds were potentially deposited by density flows triggered by strong sediment influx at the river mouth.

For deposits associated with facies 2, the grading and clast imbrication suggest bedload transport in a continuous flow with variable discharge while the concave–oblique contact suggests a channel form. The high sand content and poor stratification in some beds is evidence of rapid sedimentation on the channel floor under the lower flow regime. These sediments prograded over fine bottomsets, and they are interpreted as distributary or chute channels. Such channels have been reported as cut-and-fill deposits at the delta plain's surface and on upper delta foreslopes (McCabe 1977; Eilertsen et al. 2011).

Unit IV: fluvial deposits

Unit IV consists of graded very coarse gravel beds (facies 1, 3–5), and massive fine sand beds (facies 7). Beds of coarse sand and imbricated gravels with subhorizontal stratifications (facies 5) are observed in all sections. The contact between the beds is conformable and mostly concave. Some beds reveal planar stratifications (facies 1) in downstream sections. Thick sand beds with trough cross-stratifications (facies 3), as well as crudely stratified and graded coarse sand and gravel (facies 4), are observed only in section E7. The total thickness of unit IV ranges from 3.4 to 4 m. Unit IV has erosive contact with the underlying unit. Boulders (>300 mm) are observed at the basal contact. The upper surface outlines the topography of the present-day terrace surface, including the modern floodplain. The section from the modern floodplain (FP4) exhibits an impressive 3 m thick sequence of coarse gravel planar beds (facies 1) capped by 50 cm of massive mud (facies 7) (Fig. 9E). Bedload sediments are imbricated and normally graded as they reach cobble and block sizes near the bottom of the unit. A *Picea* sp. log dated at 4670 ± 140 cal. years BP (ULA-3041) was found at the interface between the upper fluvial unit and delta bottomset (unit II).

Interpretation

Thick sand beds with trough cross-stratifications result from the migration of dunes (Bridge 1997), which are very common in bars and channel fills in mixed-load fluvial environments (Miall 1978, 2006; Lunt et al. 2004). In section E7, their association with underlying boulder lags suggests the infill of a channel (Fig. 8C). Mixed-load fluvial environments were associated with delta and outwash plain distributaries in the classification of alluvial channels based on load characteristics (Galloway 1981; Schumm 1985; Miall 2006).

Imbricated and graded gravels with crude subhorizontal stratifications (facies 5) suggest bedload transport by highly variable currents. In sections E8 and E9, the variable grain size and multiple bedding orientations might originate from the erosion of adjacent bars during subsequent episodes of high flow. Such facies are typically formed in braided gravel-bed and outwash plain rivers (Miall 1985, 2010; Ashmore 1991). The internal structure and the absence of mud deposits in the upper sections (E8, E9) suggest the development of a dynamic river system characterized by unsteady flow, high sediment discharge, and highly mobile channels. These characteristics have been used to describe braided gravel-bed rivers in a periglacial environment (Ashworth and

Fig. 8. (A) Stratigraphic logs from section W7. (B) Imbricated and clast-supported gravels (facies 4) represent aggradation on the upper surface of a mid-channel or lateral bank; (C) the fluvial deposit (unit IV) is delimited below by a stratified deposit with boulder-sized sediment of variable thickness; (D, E) upper and lower foreset beds. (See Fig. 5 for the legend.)

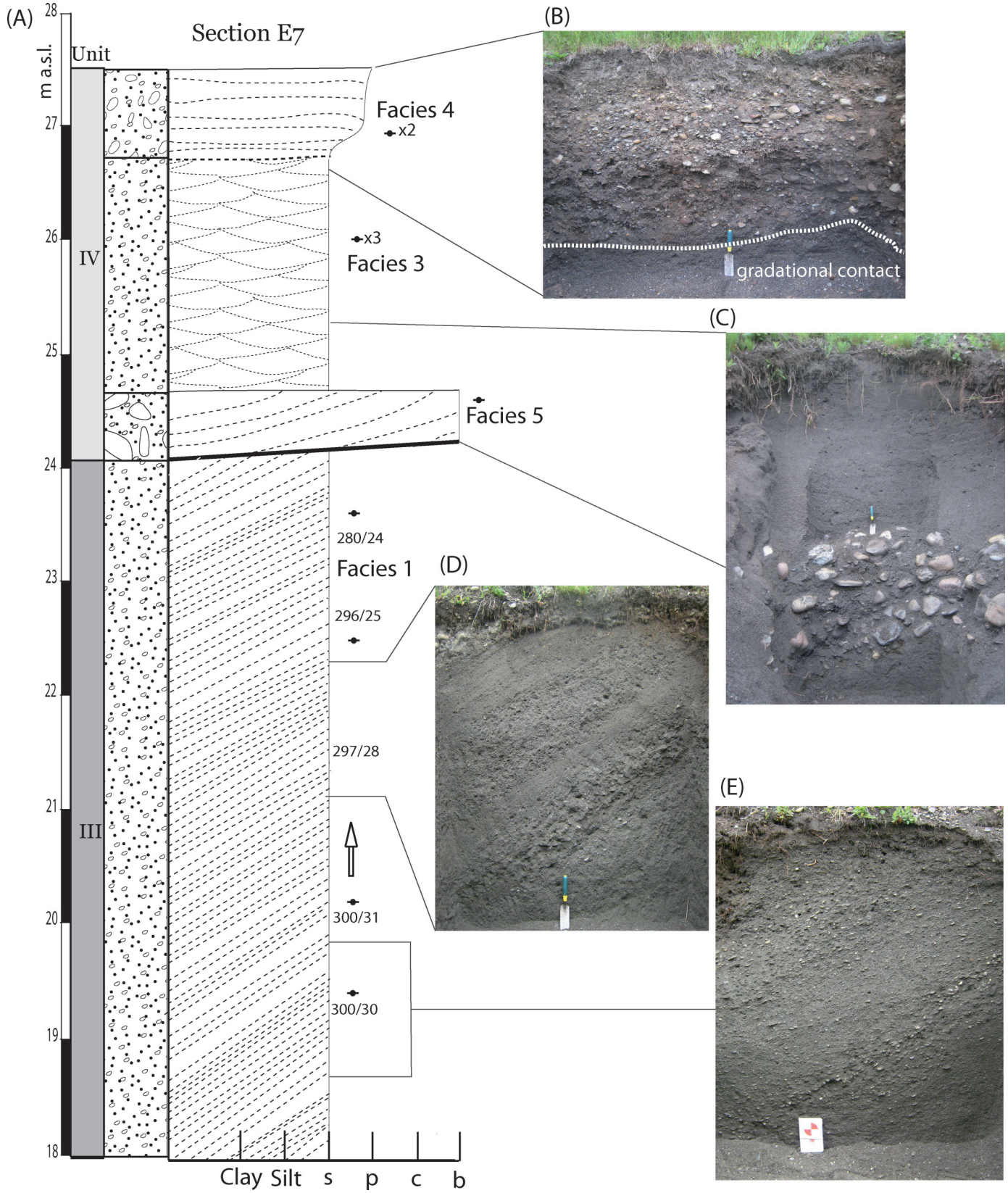

Can. J. Earth Sci. Downloaded from www.nrcresearchpress.com by Université du Québec à Rimouski on 01/02/14
For personal use only.

Can. J. Earth Sci. Downloaded from www.nrcresearchpress.com by Université du Québec à Rimouski on 01/02/14
For personal use only.

Fig. 9. Stratigraphic logs from sections (A) W1, (B) W3, (C) E6, (D) E9, and (E) FP4. Fluvial deposits (unit IV) is characterized by multiple facies: massive fine sand (facies 7); planar stratified gravel (facies 1); imbricated stratified gravel (facies 5) (See Fig. 5 for the legend.)

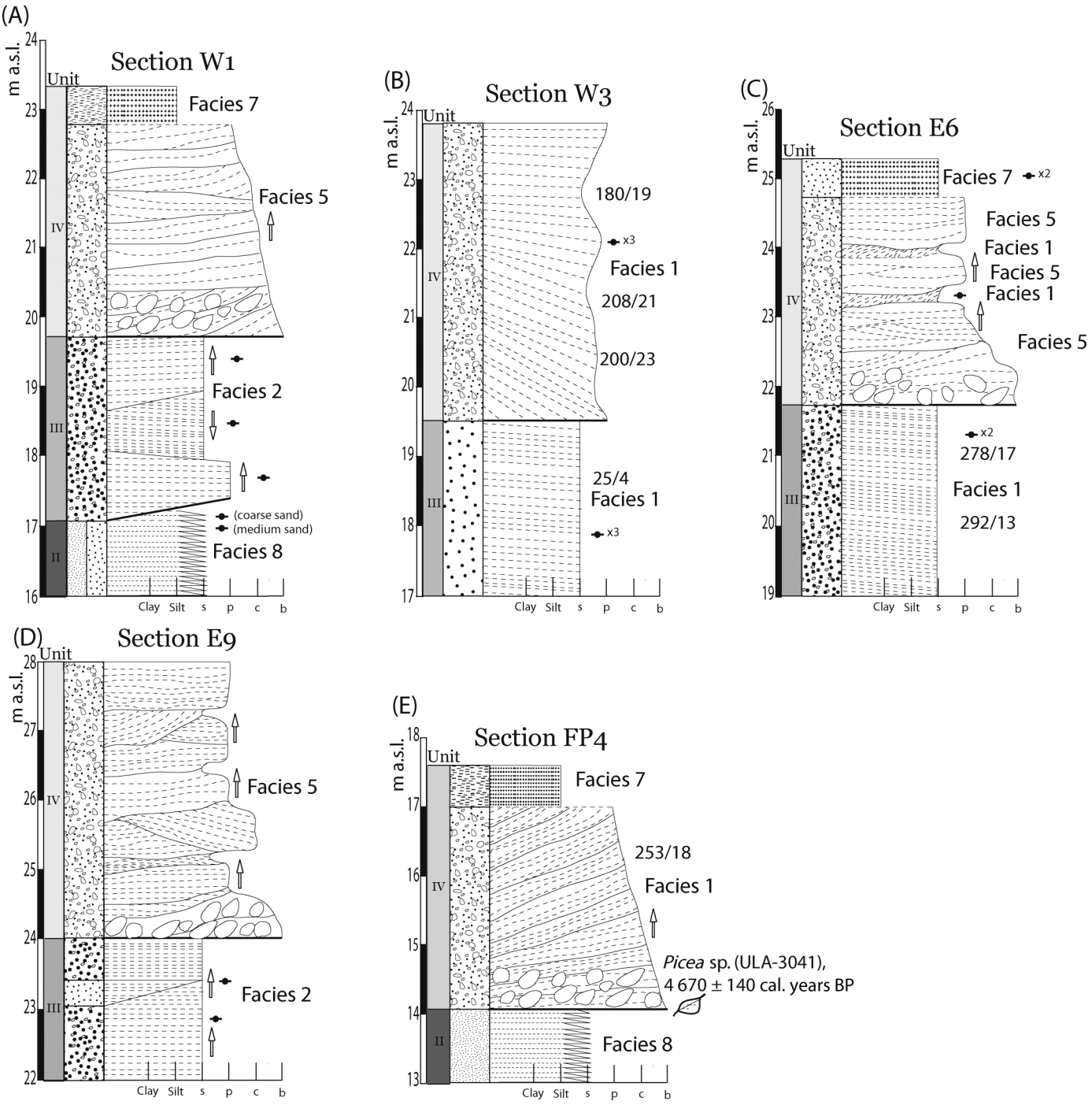

Ferguson 1986; Goff and Ashmore 1994; Rice et al. 2009). Overall, unit IV in upstream sections (E7–E9) suggests a change in the Matane River dynamics, from a mixed-load to bedload fluvial environment.

Coarse gravel beds with planar stratifications (facies 1), as observed in section W3 (Fig. 9B), could refer to fluvial load accreted laterally on the downstream portion of a channel bar (Hein and Walker 1977; Yagishita and Jopling 1983). In section FP4, planar beds are oriented perpendicular to the modern Matane River flow direction and could result from lateral accretion. Massive mud (facies 7) upon coarse gravel beds also illustrates a drastic change in the river's dynamic. Bedload transport was substituted by suspension-fallout deposition. Massive mud (facies 7) is interpreted as overbank flood deposits.

Geochemical results

Thirty-seven sediment samples were collected from units II, III, and IV. Elemental (C and N contents) and carbon stable isotope ($\delta^{13}C$) analyses were performed. Results indicate very low nitrogen contents, ranging between 0.05% and 0.35%. The stable isotope data and elemental ratios are presented and interpreted according to their inferred depositional environments (Fig. 10).

Units II, III, and IV present similar $\delta^{13}C$ values (Table 3). Neither vertical nor horizontal trends within units were observed. Values

Can. J. Earth Sci. Downloaded from www.nrcresearchpress.com by Université du Québec à Rimouski on 01/02/14
For personal use only.

Fig. 10. Typical $\delta^{13}C$ (‰) and C/N ranges for organic inputs to coastal environments (modified from Lamb et al. 2006), with data obtained from this study and classified by depositional environment. DOC, dissolved organic carbon; POC, particulate organic carbon.

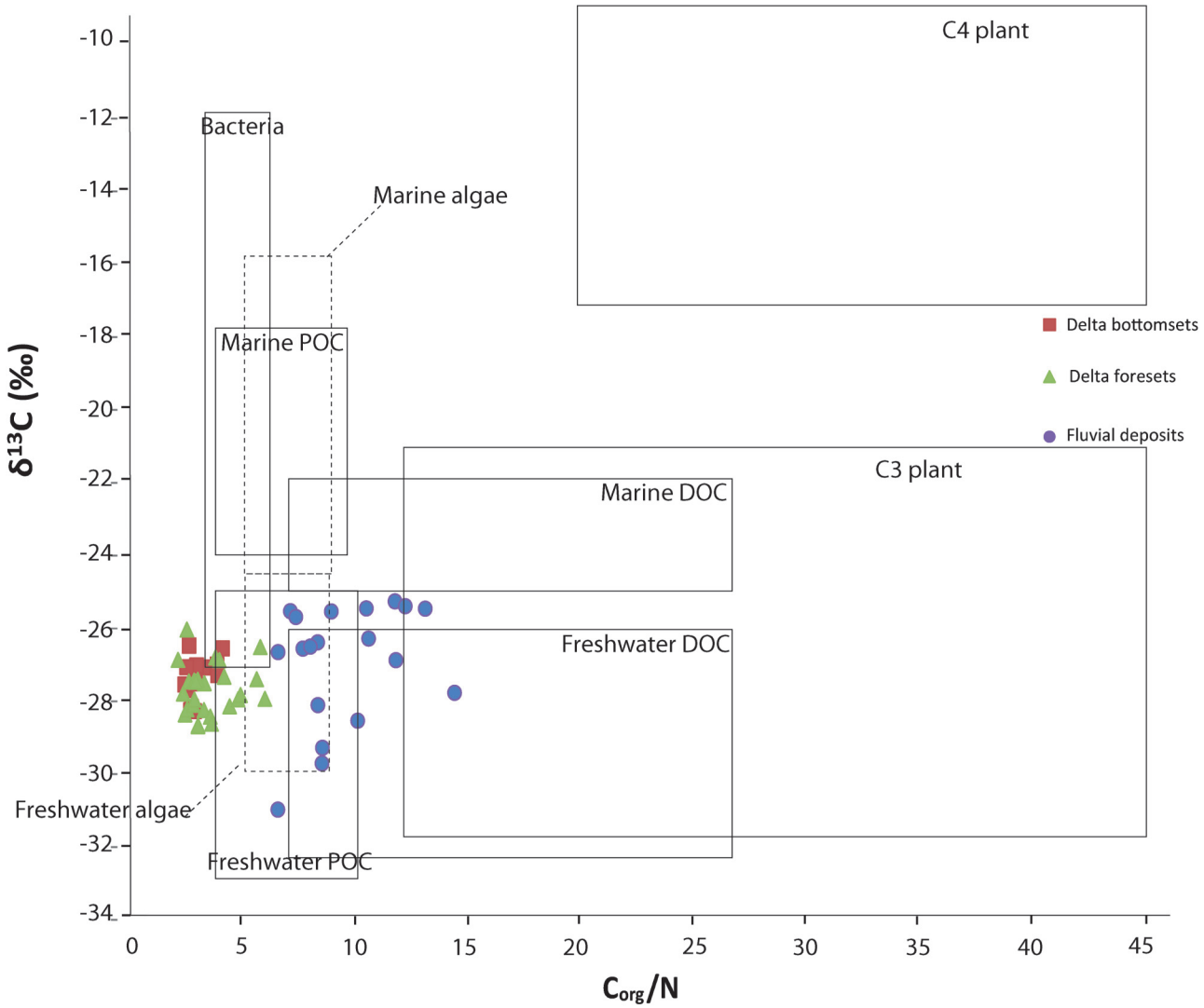

Table 3. $\delta^{13}C$ (‰) and C/N values classified by stratigraphic units.

		$\delta^{13}C/^{12}C$			C/N		
Unit	*n*	Average	Median	SD	Average	Median	SD
II	13	–27.38	–27.28	0.60	3.54	3.38	0.56
III	16	–27.54	–27.44	0.85	4.94	4.22	1.76
IV	19	–27.18	–26.87	1.71	9.14	8.95	2.61

Note: *n*, number of samples; SD, standard deviation.

of $\delta^{13}C$ around –27‰ have been reported for riverine and estuarine environments (e.g., Middelburg and Nieuwenhuize 1998; St-Onge and Hillaire-Marcel 2001; Zhang et al. 2007). Lower $\delta^{13}C$ values generally refer to terrigenous organic matter inputs from C3 pathway plants or freshwater particulate organic carbon (POC) and dissolved organic carbon (DOC) (Lamb et al. 2006). Values around –28‰ are also reported from marine algae in glacial environments (Rau et al. 1989; Meyers 1997). The absence of a gradient between distinct depositional environments in the Matane River Valley could be explained by the multiple sources of organic content with differing $\delta^{13}C$ values and efficient sediment mixing in the basin zone, as reported by Graham et al. (2001) for estuarine environments. In such settings, distinguishing depositional environments based solely on $\delta^{13}C$ values becomes difficult. The combination of C/N ratios can thus improve the understanding of the organic matter sources.

Depositional units show significant difference in their C/N ratios (Table 3). The prodeltaic deposit (unit II) bears the signature of algae inputs. Algae typically have C/N ratios between 4 and 10, while vascular plants have ratios of 20 and greater (Meyers 1997). The C/N ratios from units III and IV are different because they reveal a greater influence of terrestrial organic input. Sediment facies and geochemical results indicate that units III and IV were deposited at the transition from a subaquatic to a fluvial environment. Data points from unit II are tightly clustered while both units III and IV have sparser distributions. The low range of C/N ratios in unit II suggests a similar organic matter source and a contemporaneous phase of deposition. It supports the scenario of a laterally uniform prodeltaic unit filling the floor of the valley basin, as revealed by the stratigraphy described in the preceding text. On the other hand, the sparse results from units III and IV are in agreement with the idea that they represent laterally limited deposits that settled in different phases of formation of the alluvial system, including both delta foresets and fluvial deposits. The stable isotope and C/N ratio values highlight the relative influence of the two end-members (algae and terrestrial plants) on the

Can. J. Earth Sci. Downloaded from www.nrcresearchpress.com by Université du Québec à Rimouski on 01/02/14
For personal use only.

sources of the organic matter in the depositional environments represented by units II and IV.

Discussion

Valley fill history

During the last glacial–interglacial transition, the Matane River Valley was the scene of significant and rapid changes, from glacier proximal to deltaic to fluvial depositional environments. These changes are recorded in the stratigraphy of the fluvial terraces shaping the landscape and are located from 8 to 10 km of the current river mouth. In this section, we combine the morphological, stratigraphic, and geochemical data to propose a model for the evolution of the lower Matane River Valley from deglaciation to present day. The model is presented as four distinct phases that have to be seen as snapshots of a system that is in continuous evolution from one phase to the next (Fig. 11). The model focusses on the investigated area, which corresponds to the upstream portion of a fjord basin.

Phase 1: deglaciation and high relative sea level (from 15 800 cal. years BP)

Lebuis and David (1977) estimated that deglaciation took place around 15 800 cal. years BP. Invasion of the Goldthwait Sea into the Matane River Valley was controlled by glacier retreat and occurred during a decline in relative sea level (Coll 1994). At that time, the Matane River Valley was a bedrock-confined fjord, similar to lower valleys of the northern Gaspé Peninsula during the pre-Holocene period (Hétu and Gray 2000). Two main depositional elements represent this period of fjord glacier: ice-contact accumulations and glaciomarine deposits. In the investigated area, the glacial outwash deposits (unit I) and the kame terraces described by Coll (1994) represent the ice-contact accumulations (Fig. 11). They were most likely deposited in subglacial and ice-margin environments. The bulk of ice-contact accumulations settled at the margin of the Appalachian plateau, while the anchored glacier tongue formed a large wave-delta. The glaciomarine sediments capping the kame terraces and the valley walls, as described by Coll (1994), represent the highest relative sea level in the valley following deglaciation. In the investigated area, glaciomarine deposits are about 2 m thick. Thicker glaciomarine deposits were found sitting on till or bedrock in the lower portions of neighbouring deglaciated valleys (Hétu and Gray 2000). This suggests that the high relative sea level was short in duration in this portion of the Matane Valley fjord and that thicker glaciomarine sequences could be observed downstream of the investigated area. In fact, thick glaciomarine sequences have been observed in the St. Lawrence Estuary and were related to the last phase of deglaciation (St-Onge et al. 2008; Duchesne et al. 2010).

Phase 2: delta progradation during the decline in relative sea level (before 11 400 cal. years BP)

Following the invasion of the Goldthwait Sea in the Matane River Valley, relative sea level started falling and highly dynamic glacial meltwater streams gave rise to low-density turbidity currents that filled the fjord with sediments. Aggradation of the basin floor reduced accommodation space and promoted delta progradation at the head of the Matane Valley fjord, as mentioned in other fjord studies (Corner et al. 1990; Eilertsen et al. 2006).

Considering the coarse grain size of the bottomsets unit (II) found in the investigated area, the head of the fjord basin was probably around 11 km up the valley, which is consistent with Dionne and Coll's (1995) estimation. The delta slope (unit III) was temporarily located around kilometre 10 (section E7, Fig. 8). The coarse grain size and the steeply inclined beds (24°–31°) suggest that unit III was part of a Gilbert-type delta (McCabe and Eyles 1988; Postma 1990). No major deformation or debris flow deposits were recorded, which indicates that it was a stream-fed delta and not an ice-contact delta (Benn and Evans 2010).

As the foreset beds generally lay between 1 and 3 m below a.s.l. (Eilertsen et al. 2011), a minimum relative sea level of 30 m above the present level can be estimated for the formation of this stream-fed delta. Based on the relative sea level curve for the Matane region (Fig. 3), formation of the Gilbert-type delta likely occurred before 11 400 cal. years BP. At that time, the delta was supplied by an alluvial system, although a glacier was still potentially active upstream in the Notre-Dame mountain area (Lebuis 1973; Prichonnet 1995). This period also corresponds to a phase of major changes in the rate of relative sea level decline in the Matane region. A marine terrace identified by Coll (1994) between 30 and 35 m a.s.l. indicates a period of relative stability or a small-scale relative sea level rise in the Matane region. Based on radiocarbon dating from Coll (1994), this period must have occurred between 10 895 ± 345 (UL-906) and 11 650 ± 450 (UL-884) cal. years BP (Fig. 2). It is possible that the same short relative sea level stability or small increase favoured the formation of a Gilbert-type delta upstream in the Matane River Valley. This same period is suggested by Hétu and Gray (2000) as the last period of fluvial delta activity in other deglaciated valleys of the northern Gaspé Peninsula.

Geochemical analyses allowed us to distinguish units II and III based on their elemental ratios (C/N). The analyses indicate a greater proportion of terrestrial organic matter in the deltaic foresets compared with the prodeltaic unit. In addition, more uniformity in the geochemical results of unit II indicates a laterally homogenous unit. The combined analysis of C/N ratios and $\delta^{13}C$ values do not prove beyond a doubt that the basin in which the delta prograded corresponded to an extension of the Goldthwait Sea. The relatively low $\delta^{13}C$ and C/N values from units II and III suggest the organic matter input was mainly from freshwater algae. However, the isotopic and elemental values of upper estuaries and fjords generally represent a mixture of organic sources from terrestrial and marine inputs (Peters et al. 1978; St-Onge and Hillaire-Marcel 2001; Lamb et al. 2006). Major glacio-fluvial or fluvial inputs could have influenced the salinity and thus the composition of aquatic organic matter present in the marine basin. More importantly, these results demonstrate the relevance of isotopic ratio analyses in the distinction and interpretation of holocene deposits.

Phase 3: fluvial sedimentation and incision with formation of upper terraces (~11 200–10 200 cal. years BP)

Fluvial incision occurred during the final phase of the relative sea level decline. Considering the relative altitude of these fluvial deposits (min–max: 19–28 m a.s.l.), it seems probable that progradation and incision of the fluvial system took place between 11 200 and 10 200 cal. years BP during the final phase of the Goldthwait Sea regression. The fluvial unit (IV) reflects highly variable local hydraulic conditions and a change in the fluvial style. Fluvial deposits at the top of the most elevated terraces (E7–E9) suggest a shift from a stream with one large channel and mixed-sediment transport to a highly mobile stream with shallow and narrow channels and high competence flow. It follows that the upper delta plain was substituted by a braided outwash plain following the drop in relative sea level. Lower terraces also show very coarse-grained sediments, but they are overlain by overbank deposits. The presence of overbank deposits suggests well-defined topographic levels in an alluvial plain (Miall 1985). The complex morphology observed at terrace surfaces suggests multiple channels with bars and islands and occasional chute channels. The absence of a clearly defined ridge and swell topography and the clear longitudinal orientation of relict channels rule out the scenario of a classic meandering river (Nicoll and Hickin 2010). The transition between upper and lower fluvial deposits in the investigated area is interpreted as a braidplain that evolved into a low sinuosity, gravel-bed river environment, as has been reported in other studies (Miall 1985). River incision eroded glacial deposits as the upper

Fig. 11. Evolution model of the Matane River Valley in four phases. Abbreviations in the inset circle: OB, overbank deposit; BL, bedload fluvial deposits; IRD, ice-rafted debris; BS, bottomsets; GO, glacial outwash deposit. RSL, relative sea level.

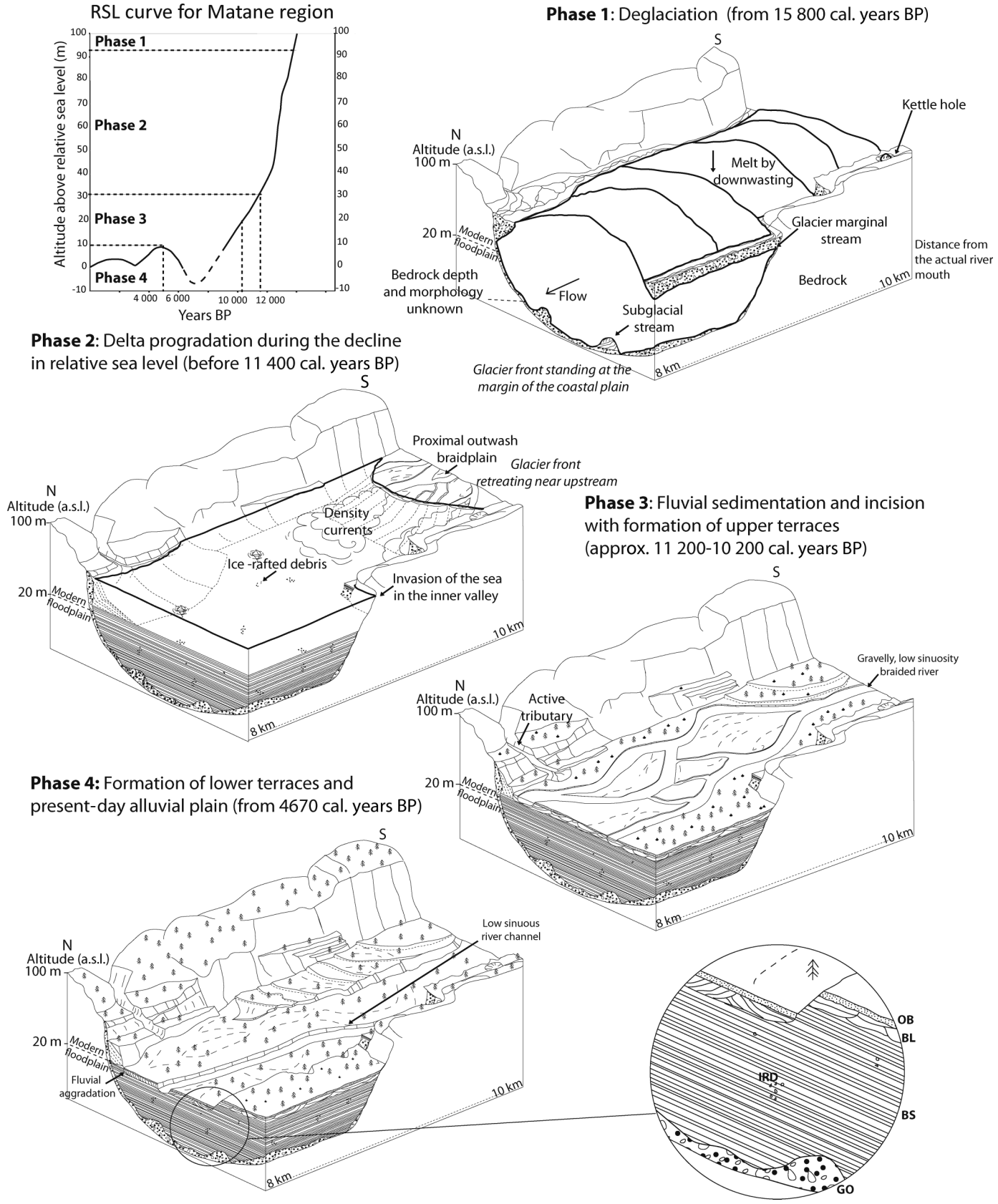

Can. J. Earth Sci. Downloaded from www.nrcresearchpress.com by Université du Québec à Rimouski on 01/02/14
For personal use only.

Can. J. Earth Sci. Downloaded from www.nrcresearchpress.com by Université du Québec à Rimouski on 01/02/14
For personal use only.

valley was slowly deglaciated. As a consequence, fluvial deposits in the terraces are composed of boulders and gravels derived from eroded glacial deposits. Gradual exhaustion of sediment sources in the upstream catchment could explain the transition between a highly mobile braided plain environment to a fluvial environment with a defined floodplain.

Phase 4: formation of lower terraces and present-day alluvial plain (from 4670 cal. years BP)

The rise of relative sea level during the Middle Holocene resulted in a new episode of aggradation of the fluvial system. The *Picea* sp. log (4670 cal. years BP) found at the interface between the bedload deposit of the modern floodplain and the delta bottomsets (unit II) was deposited after the Laurentian transgression that followed a relative sea level low stand (Dionne and Coll 1995). This transgression formed the Mic-Mac terrace on the south shore of St. Lawrence Estuary (Dionne 1997). In the Matane area, relative sea level increased ~10 m a.s.l. from 7000 to 5000 cal. years BP (Dionne and Coll 1995). In the investigated area, the 3 m modern floodplain was deposited after 4670 ± 140 cal. years BP during the highstand phase of the Laurentian transgression. This supports the idea of Hétu and Gray (2002) that alluvial floodplains in valleys of the northern Gaspé Peninsula are very sensitive to relative sea level fluctuations. For example, they demonstrate that the Cap-Chat River Valley was filled by fluvial deposits up to 5 km upstream during the same mid-Holocene Laurentian transgression. The time gap between the onset of the Laurentian transgression and the aggradation of the modern Matane River floodplain in the investigated area demonstrates that relative sea level fluctuations had delayed morphological impacts on the upstream portion of this alluvial system. It also shows that fluvial deposits from an environment affected by several relative sea level fluctuations can appear as anachronous deposits and not a single regressive unit.

Applications of fjord-valley models

Ice-contact accumulations and glaciomarine deposits are described as part of the deglacial transgressive systems tracts in Corner's (2006) fjord-valley fill model. They are found locally as pockets of sorted sediment overlying bedrock and on valley walls. Kame terrace surfaces capped by glaciomarine clay represent the maximum flooding surface described in Hansen's (2004) fjord-valley model. The upper boundary of the glacial outwash deposits as well as the kame terrace surface in the Matane River Valley correspond to the deglaciation flooding surface.

Deltaic deposits are included in the deglacial highstand and postglacial forced regressive system tracts in Corner's (2006) conceptual fjord-valley fill model. According to Corner (2006), the distinction between both system tracts relies on the identification of glacially influenced and non-glacially influenced lithofacies and geometry. The only potential evidence of changes between both environments is found in one section (W2; Fig. 6), where the coarse-grained graded beds grade into fine-grained graded beds. The coarse graded beds contain numerous dropstones and numerous synsedimentary deformations, which suggest intense ice rafting and underflow current activity. The fine-grained graded beds contain no dropstone and only a few deformations (wavy bedding), suggesting (*i*) calmer hydrodynamic conditions that allowed fine sediments to settle by gravity, (*ii*) a lower rate of sediment supply, and (*iii*) less ice rafting activity. This change of facies within unit II could represent the boundary between glacial and non-glacial influence in the fjord basin.

Unit IV represents fluvial deposits that overlie (by the action of erosion) older deposits in a series of extensive terraces. It is described in Corner's fjord-valley fill model (2006) as part of the postglacial forced-regressive systems tracts. The falling relative sea level produces a single fluvial unit that is equal to or thinner than the channel depth, which was between 3.5 and 4 m in the Matane River Valley. The rapid vertical incision of river channels during phase 3 prevented the deltaic deposit from being more extensively eroded by fluvial processes.

Together, the deltaic and fluvial deposits represented by units II, III, and IV were formed during a phase of relative sea level decline in the St. Lawrence Estuary. They are described in the postglacial forced-regressive systems tracts of Corner's (2006) fjord-valley fill model as the major filling unit in the fjord valley.

Conclusion

Four distinct phases of formation of the modern alluvial system in the Matane River Valley have been highlighted by stratigraphic and morphological analyses. Glacial outwash deposits (unit I) and kame terraces represent the glacier stage. Sparse glaciomarine sediments found at the top of the kame terraces in the investigated area highlight the fact that transgression must have been short in the upstream portion of the fjord. Both ice-contact accumulations and glaciomarine deposits represent the deglacial transgressive systems tracts described in fjord-valley models. Delta bottomsets (unit II) represents the bulk of the fjord basin fill and were fed by glacier melt streams. High sediment yield and relative decline in sea level induces a reduction of accommodation space in the fjord basin. Temporary relative sea level stability or a small increase could have influenced the formation of a Gilbert-type delta in the upstream portion of the fjord as well as the incision of a marine terrace on the coastal plain. As relative sea level continued to fall, the upper delta plain emerged and evolved into an outwash braidplain. Gradual exhaustion of sediment sources in the upstream catchment must have influenced sediment yields and flooding patterns, allowing a distinct floodplain to form upon the alluvial system. Both deltaic and fluvial units represent the major filling units of the upstream portion of the fjord basin in the Matane River Valley. They represent postglacial forced-regressive systems tracts described in fjord-valley models as the major part of fjord-valley fill.

The geochemical and stable isotope analyses provided complementary insight into the depositional environments. Even though the absolute values could not be used to precisely determine the source of the organic matter in the sediment, they illustrate that specific depositional environments share a similar isotopic and elemental signature, further supporting our description and interpretation of the lithofacies. It could also allow a comparison of the isotopic signatures of similar deposits in neighbouring deglaciated valleys, thus extending the application of the fjord-valley model to the northern Gaspé Peninsula. Further investigation should be made concerning the influence of basin morphology on the spatial pattern of regressive deposits, especially on the distribution, burial depth, and thickness of the unit's facies. Drilling and seismic profiling would be required to define the different boundaries of Matane River Valley deposits, especially the depth of the delta bottomsets and the morphology of the bedrock surface.

Acknowledgements

This study was completed as part of a Master of Science degree by J.-P.M. at the Université du Québec à Rimouski (UQAR) and was funded by the Natural Sciences and Engineering Research Council of Canada (NSERC) and the Fonds de recherche du Québec – Nature et technologies grants. UQAR and the Institut des Sciences de la Mer de Rimouski (ISMER) provided use of the sedimentology laboratory. We are grateful to A. Morissette, M. Babin, C. Belzile, and C. Renault for their support in the sedimentology laboratory and to J. Bérubé, A. Lelièvre Mathieu, C.A. Cloutier, A. Montane, S. Demers, J. Dubé, V. Parent, and T. Olsen of the Laboratoire de géomorphologie et dynamique fluvial de l'UQAR for their field assistance and valuable discussions. We greatly appreciate comments from L. Hansen and P. Lajeunesse on earlier versions of the manuscript. Laure Devine revised the English.

Can. J. Earth Sci. Downloaded from www.nrcresearchpress.com by Université du Québec à Rimouski on 01/02/14
For personal use only.

References

Abreu, V.S., and Anderson, J.B. 1998. Glacial eustasy during the Cenozoic: sequence stratigraphic implications. American Association of Petroleum Geologists Bulletin, **82**(7): 1385–1400.

Ashley, G.M. 1975. Rhythmic sedimentation in glacial Lake Hitchcock, Massachusetts-Connecticut. *In* Glaciofluvial and glaciolacustrine sedimentation. *Edited by* A. V. Jopling, and B. C. McDonald. Society of Economic Paleontologists and Mineralogists, Special Publication, **23**, pp. 304–320.

Ashmore, P. 1991. Channel Morphology and Bed Load Pulses in Braided, Gravel-Bed Streams. Geografiska Annaler, Series A, Physical Geography, **73**(1): 37–52. doi:10.2307/521212.

Ashworth, P.J., and Ferguson, R.I. 1986. Interrelationships of channel processes, changes and sediments in a proglacial braided river. Geografiska Annaler, Series A, Physical Geography, **68**(4): 361–371. doi:10.2307/521527.

Benn, D.I., and Evans, D.J.A. 2010. Glaciers and glaciation. Hodder Education, London.

Blott, S.J., and Pye, K. 2001. Gradistat, a grain distribution and statistics package for the analysis of unconsolidated sediments. Earth Surface Processes and Landforms, **26**: 1237–1248. doi:10.1002/esp.261.

Blum, M.D., and Törnqvist, T. 2000. Fluvial responses to climate and sea-level change: a review and look forward. Sedimentology, **47**(1): 2–48. doi:10.1046/j.1365-3091.2000.00008.x.

Bouma, A.H. 1962. Sedimentology of some flysch deposits: a graphic approach to facies interpretation. Elsevier, New York.

Bridge, J.S. 1997. Thickness of sets of cross strata and planar strata as a function of formative bedwave geometry and migration, and aggradation rate. Geology, **25**: 971–974. doi:10.1130/0091-7613(1997)025<0971:TOSOCS>2.3.CO;2.

Chauvin, L. 1977. Étude sédimentologique des dépôts glacio-estuariens de la vallée de la rivière Saint-Anne, Gaspésie. M.Sc. thesis, Department of Geography, Université de Montréal, Montréal, Qc.

Coll, D. 1994. Aperçu géomorphologique du Quaternaire de la vallée inférieure de la Matane. M. Sc. thesis, Department of Geography, Université Laval, Québec, Qc.

Corner, G.D. 2006. A transgressive-regressive model of fjord valley fill: stratigraphy, facies and depositional controls. *In* Incised valleys in time and space. *Edited by* R.W. Dalrymple, D.A. Leckie, and R.W. Tilan. Special Publications of the Society for Sedimentary Geology, **85**, pp. 161–178.

Corner, G.D., Nordahl, E., Munch-Ellingsen, K., and Robertsen, K.R. 1990. Morphology and sedimentology of an emergent fjord-head Gilbert type delta: Alta delta, Norway. *In* Coarse-grained deltas. *Edited by* A. Colella and D.B. Prior. Special Publication of the International Association of Sedimentologist, **10**, pp. 55–168.

Dionne, J.-C. 1977. La mer de Goldthwait au Québec. Géographie physique et Quaternaire, **31**(1): 61–80. doi:10.7202/1000055ar.

Dionne, J.-C. 1997. Nouvelles données sur la transgression Laurentienne, côte sud du moyen estuaire du Saint-Laurent, Québec. Géographie physique et Quaternaire, **51**(2): 201–210. doi:10.7202/033118ar.

Dionne, J.-C., and Coll, D. 1995. Le niveau marin relatif dans la région de Matane (Québec), de la déglaciation à nos jours. Géographie physique et Quaternaire, **49**(3): 363–380. doi:10.7202/033060ar.

Duchesne, M.J., Pinet, N., Bédard, K., St-Onge, G., Lajeunesse, P., Campbell, C., and Bolduc, A. 2010. Role of the bedrock topography in the Quaternary filling of a giant semi-enclosed basin: the Lower St. Lawrence Estuary, Eastern Canada. Basin Research, **22**: 933–951. doi:10.1111/j.1365-2117.2009.00457.x.

Eilertsen, R.S., Corner, G.D., Aasheim, O., Andreassen, K., Kristoffersen, Y., and Ystborg, H. 2006. Valley-fill stratigraphy and evolution of the Malselv fjord valley, Northern Norway. *In* Incised valleys in time and space. *Edited by* R.W. Dalrymple, D.A. Leckie, and R.W. Tilan. Special Publications of the Society for Sedimentary Geology, **85**, pp. 179–195.

Eilertsen, R.S., Corner, G.D., Aasheim, O., and Hansen, L. 2011. Facies characteristics and architecture related to paleodepth of Holocene fjord-delta sediments. Sedimentology, **58**: 1784–1809. doi:10.111/j.1365-3091.2011.01239.x.

Fiore, J., Pugin, A., and Beres, M. 2002. Sedimentological and GPR studies of subglacial deposits in the Joux Valley (Vaud, Switzerland): backset accretion in an esker followed by an erosive jökulhlaup. Géographie physique et Quaternaire, **56**(1): 19–32. doi:10.7202/008602ar.

Fisk, H.N. 1944. Geological Investigation of the Alluvial Valley of the Lower Mississippi River: Vicksburg, MS, Mississippi River Commission.

Forwick, M., and Vorren, T.O. 2011. Stratigraphy and deglaciation of the Isfjorden area, Spitsbergen. Norwegian Journal of Geology, **90**: 163–179.

Galloway, W.E. 1981. Depositional architecture of Cenozoic Gulf coastal plain fluvial systems. The Society of Economic Paleontologists and Mineralogists Special Publication, **31**: 127–155.

Goff, J.R., and Ashmore, P. 1994. Gravel transport and morphological change in braided Sunwapta River, Alberta, Canada. Earth Surface Processes and Landforms, **19**: 195–212. doi:10.1002/esp.3290190302.

Graham, M.C., Eaves, M.A., Farmer, J.G., Dobson, J., and Fallick, A.E. 2001. A study of carbon and nitrogen stable isotope and elemental ratios as potential indicators of source and fate of organic matter in sediments of the Forth Estuary, Scotland. Estuarine, Coastal and Shelf Science, **51**: 375–380. doi:10.1006/ecss.2000.0742.

Gray, J.T., and Hétu, B. 1987. Delta et flèche littorale à Rivière-La-Madeleine. *In* Processus et paléo-environnements du Quaternaire dans la péninsule gaspésienne et dans le Bas-Saint-Laurent. *Edited by* J.T. Gray, XII INQUA International meeting, CNRC. pp. 50–52.

Hansen, L. 2004. Deltaic infill of a deglaciated arctic fjord, east Greenland: sedimentary facies and sequence stratigraphy. Journal of Sedimentary Research, **74**(3): 422–437. doi:10.1306/102703740422.

Hansen, L., Beylich, A., Burki, V., Fredin, O., Larsen, E., Lysa, A., Nesje, A., Stalsberg, K., and Tønnesen, J.F. 2009. Stratigraphic architecture and infill history of a deglaciated bedrock valley based on georadar, seismic profiling and drilling. Sedimentology, **56**: 1751–1773. doi:10.1111/j.1365-3091.2009.01056.x.

Hein, F.J., and Walker, R.G. 1977. Bar evolution and development of stratification in the gravelly, braided, Kicking Horse River, British Columbia. Canadian Journal of Earth Science, **14**(4): 561–570. doi:10.1139/e77-058.

Heinz, J., Kleineidam, S., Teutsch, G., and Aigner, T. 2003. Heterogeneity patterns of Quaternary glaciofluvial gravel bodies (S-W Germany): application for hydrogeology. Sedimentary Geology, **158**: 1–23. doi:10.1016/S0037-0738(02)00239-7.

Hétu, B. 1994. Déglaciation, émersion des terres et pergélisol tardiglaciaire dans la région de Rimouski, Québec. Paléo-Québec, **22**: 5–48.

Hétu, B., and Gray, J.T. 2000. Les étapes de la déglaciation dans le nord de la Gaspésie (Québec, Canada) : les marges glaciaires des Dryas ancien et récent. Géographie physique et Quaternaire, **54**(1): 5–40. doi:10.7202/004831ar.

Hétu, B., and Gray, J.T. 2002. L'apport de la géomorphologie à l'archéologie des périodes paléoindienne et archaïque dans l'est du Québec. Recherches amérindiennes au Québec, **33**(3): 76–90.

Kostic, B., Becht, A., and Aigner, T. 2005. 3-D sedimentary architecture of a Quaternary gravel delta (S-W Germany): implications for hydrostratigraphy. Sedimentary Geology, **181**: 143–171. doi:10.1016/j.sedgeo.2005.07.004.

Lamb, A.L., Wilson, G.P., and Leng, M.J. 2006. A review of coastal palaeoclimate and relative sea-level reconstructions using δ13C and C/N ratios in organic material. Earth Science Reviews, **75**: 29–57. doi:10.1016/j.earscirev.2005.10.003.

Lebuis, J. 1973. Géologie du Quaternaire de la région de Matane-Amqui, comtés de Matane et Matapédia, Preliminary Survey DP 216, Government of Quebec, Qc.

Lebuis, J., and David, P.P. 1977. La stratigraphie et les événements du Quaternaire de la partie occidentale de la Gaspésie, Québec. Géographie physique et Quaternaire, **31**(3–4): 275–296. doi:10.7202/1000278ar.

Longva, O., and Bakkejord, K.J. 1990. Iceberg deformation and erosion in soft sediments, Southeast Norway. Marine Geology, **92**: 87–104. doi:10.1016/0025-3227(90)90028-I.

Lunt, I.A., Bridge, J.S., and Tye, R.S. 2004. A quantitative, three-dimensional model of gravelly braided rivers. Sedimentology, **51**: 377–414. doi:10.1111/j.13653091.2004.00627.x.

McCabe, A.M. 1977. Deep distributary channels and giant bedforms in the Upper Carboniferous of the Central Pennines, northern England. Sedimentology, **4**(2): 271–290. doi:10.1111/j.1365-3091.1977.tb00257.x.

McCabe, A.M., and Eyles, N. 1988. Sedimentology of an ice-contact glaciomarine delta, Carey Valley, Northern Ireland. Sedimentary Geology, **59**: 1–14. doi:10.1016/0037-0738(88)90097-8.

McNeely, R., Dyke, A.S., and Southon, J.R. 2006. Canadian marine reservoir ages. Preliminary data assessment open file 5049, Geological Survey of Canada, Ottawa.

Meyers, P.A. 1997. Organic geochemical proxies of paleoceanographic, paleolimnologic and paleoclimatic processes. Organic Geochemistry, **27**(5–6): 213–250. doi:10.1016/S0146-6380(97)00049-1.

Miall, A.D. 1978. Lithofacies types and vertical profile models in braided river deposits: a summary. *In* Fluvial sedimentology V. *Edited by* A.D. Miall. American Association of Petroleum Geologists, pp. 597–604.

Miall, A.D. 1985. Architectural-element analysis: a new method of facies analysis applied to fluvial deposits. Earth Science Reviews, **22**: 261–308. doi:10.1016/0012-8252(85)90001-7.

Miall, A.D. 2006. Geology of fluvial deposits, sedimentary facies, basin analysis and petroleum geology. Springer Link Publications, Berlin.

Miall, A.D. 2010. Alluvial deposits. *In* Facies models 4. *Edited by* N.P. James and R.W. Dalrymple. Geological Association of Canada, pp. 105–138.

Middelburg, J.J., and Nieuwenhuize, J. 1998. Carbon and nitrogen stable isotopes in suspended matter and sediments from the Schelde Estuary. Marine Chemistry, **60**: 217–225. doi:10.1016/S0304-4203(97)00104-7.

Middleton, G.V. 1993. Sediment deposition from turbidity currents. Annual Review of Earth and Planetary Sciences, **21**: 89–114. doi:10.1146/annurev.ea.21.050193.000513.

Nemec, W. 1990. Aspects of sediment movement on steep delta slopes. *In* Coarse-grained deltas. *Edited by* A. Colella and D.B. Prior. Special Publication of the International Association of Sedimentologists, **10**, pp. 29–73.

Nicoll, T.J., and Hickin, E.J. 2010. Planform geometry and channel migration of confined meandering rivers on the Canadian prairies. Geomorphology, **116**: 37–47. doi:10.1016/j. geomorph.2009.10.005.

Occhietti, S., and Richard, P.J.H. 2003. Effet réservoir sur les âges ^{14}C de la Mer de Champlain à la transition pléisotcène-holocène: révision de la chronologie de la déglaciation au Québec méridional. Géographie physique et Quaternaire, **57**(2–3): 115–138. doi:10.7202/011308ar.

Ollerenshaw, N.C. 1967. Région de Cuoq-Langis, comtés de Matapédia et de Matane. Geological report 121, Government of Quebec, Qc.

Peters, K.E., Sweeney, R.E., and Kaplan, I.R. 1978. Correlation of carbon and nitrogen stable isotope ratios in sedimentary organic matter. Limnology and Oceanography, **23**(4): 598–604. doi:10.4319/lo.1978.23.4.0598.

Pisarska-Jamrozy, M., and Weckwerth, P. 2012. Soft-sediment deformation structures in a Pleistocene glaciolacustrine delta and their implications for the recognition of subenvironments in delta deposits. Sedimentology, **60**(3): 637–665. doi:10.1111/j.1365-3091.2012.01354.x.

Postma, G. 1990. Depositional architecture and facies of river and fan deltas: a synthesis. *In* Coarse-grained deltas. *Edited by* A. Colella and D. B. Prior. Special Publication of the International Association of Sedimentologists, **10**, pp. 13–27.

Prichonnet, G. 1995. Géologie et géochronologie postglaciaire dans la région limitrophe de la Gaspésie et du Bas-Saint-Laurent, Québec. Geological Survey of Canada, no. 488.

Rau, G.H., Takahashi, T., and Des Marais, D.J. 1989. Latitudinal variations in plankton $\delta^{13}C$: implications for CO_2 and productivity in past oceans. Nature, **341**(6242): 516–518. doi:10.1038/341516a0. PMID:11536614.

Rice, S.P., Church, M., Wooldridge, C.L., and Hickin, E.J. 2009. Morphology and evolution of bars in a wandering gravel-bed river; lower Fraser River, British Columbia, Canada. Sedimentology, **56**: 709–736. doi:10.1111/j.1365-3091.2008.00994.x.

Rust, B.R. 1972. Structure and process in a braided river. Sedimentology, **18**: 221–245. doi:10.1111/j.1365-3091.1972.tb00013.x.

Sandgren, P. 1983. The deglaciation of the Klippan area, southern Sweden. Ph.D. Thesis, Department of Quaternary Geology, Lund University, Sweden.

Schumm, S.A. 1985. Patterns of alluvial rivers. Annual Review of Earth and Planetary Sciences, **13**: 5–27. doi:10.1146/annurev.ea.13.050185.000253.

Shaw, J., and Gorrell, G. 1991. Subglacially formed dunes with bimodal and graded gravel in the Trenton Drumlin Field, Ontario. Géographie physique et Quaternaire, **45**(1): 21–34. doi:10.7202/032842ar.

St-Onge, G., and Hillaire-Marcel, C. 2001. Isotopic constraints of sedimentary inputs and organic carbon burial rates in the Saguenay Fjord, Quebec. Marine Geology, **176**: 1–22. doi:10.1016/S0025-3227(01)00150-5.

St-Onge, G., Lajeunesse, P., Duchesne, M.J., and Gagné, H. 2008. Identification and dating of a key Late Pleistocene stratigraphic unit in the St. Lawrence Estuary and Gulf (Eastern Canada). Quaternary Science Reviews, **27**: 2390–2400. doi:10.1016/j.quascirev. 2008.08.023.

Veillette, J. 1986. Former southwesterly ice flows in the Abitibi-Temiskaming region: implications for the configuration of the late Wisconsinan ice sheet. Canadian Journal of Earth Sciences, **23**(11): 1724–1741. doi:10.1139/e86-159.

Wilson, G.P., Lamb, A.L., Leng, M.J., Gonzalez, S., and Huddart, D. 2005. $\delta^{13}C$ and C/N as potential coastal palaeoenvironmental indicators in the Mersey Estuary, UK. Quaternary Science Reviews, **24**: 2015–2029. doi:10.1016/j.quascirev.2004.11.014.

Yagishita, K., and Jopling, A.V. 1983. Grain fabric of planar cross-bedding formed by lateral accretion, Caledon Outwash, Ontario, Canada. The Journal of Geology, **91**(5): 599–606. doi:10.1086/628807.

Zhang, J., Wu, Y., Jennerjahn, T.C., Ittekkot, V., and He, Q. 2007. Distribution of organic matter in the Changjiang (Yangtze River) Estuary and their stable carbon and nitrogen isotopic ratios: implications for source discrimination and sedimentary dynamics. Marine Chemistry, **107**: 111–126. doi:10.1016/j.marchem.2007.02.003.

Can. J. Earth Sci. Downloaded from www.nrcresearchpress.com by Université du Québec à Rimouski on 01/02/14
For personal use only.